Original Article

MOLECULAR METABOLISM

Hepatic Activin E mediates liver-adipose inter-organ communication, suppressing adipose lipolysis in response to elevated serum fatty acids

John D. Griffin*, Joanne M. Buxton, Jeffrey A. Culver, Robert Barnes, Emily A. Jordan, Alexis R. White, Stephen E. Flaherty, Barbara Bernardo, Trenton Ross, Kendra K. Bence, Morris J. Birnbaum

ABSTRACT

Objective: The liver is a central regulator of energy metabolism exerting its influence both through intrinsic processing of substrates such as glucose and fatty acid as well as by secreting endocrine factors, known as hepatokines, which influence metabolism in peripheral tissues. Human genome wide association studies indicate that a predicted loss-of-function variant in the Inhibin βE gene (*INHBE),* encoding the putative hepatokine Activin E, is associated with reduced abdominal fat mass and cardiometabolic disease risk. However, the regulation of hepatic Activin E and the influence of Activin E on adiposity and metabolic disease are not well understood. Here, we examine the relationship between hepatic Activin E and adipose metabolism, testing the hypothesis that Activin E functions as part of a liver-adipose, inter-organ feedback loop to suppress adipose tissue lipolysis in response to elevated serum fatty acids and hepatic fatty acid exposure.

Methods: The relationship between hepatic Activin E and non-esterified fatty acids (NEFA) released from adipose lipolysis was assessed *in vivo* using fasted CL 316,243 treated mice and *in vitro* using Huh7 hepatocytes treated with fatty acids. The influence of Activin E on adipose lipolysis was examined using a combination of *Inhbe* knockout mice, a mouse model of hepatocyte-specific overexpression of Activin E, and mouse brown adipocytes treated with Activin E enriched media.

Results: Increasing hepatocyte NEFA exposure *in vivo* by inducing adipose lipolysis through fasting or CL 316,243 treatment increased hepatic *Inhbe* expression. Similarly, incubation of Huh7 human hepatocytes with fatty acids increased expression of *INHBE*. Genetic ablation of *Inhbe* in mice increased fasting circulating NEFA and hepatic triglyceride accumulation. Treatment of mouse brown adipocytes with Activin E conditioned media and overexpression of Activin E in mice suppressed adipose lipolysis and reduced serum FFA levels, respectively. The suppressive effects of Activin E on lipolysis were lost in CRISPR-mediated ALK7 deficient cells and ALK7 kinase deficient mice. Disruption of the Activin E-ALK7 signaling axis in *Inhbe* KO mice reduced adiposity upon HFD feeding, but caused hepatic steatosis and insulin resistance.

Conclusions: Taken together, our data suggest that Activin E functions as part of a liver-adipose feedback loop, such that in response to increased serum free fatty acids and elevated hepatic triglyceride, Activin E is released from hepatocytes and signals in adipose through ALK7 to suppress lipolysis, thereby reducing free fatty acid efflux to the liver and preventing excessive hepatic lipid accumulation. We find that disrupting this Activin E-ALK7 inter-organ communication network by ablation of *Inhbe* in mice increases lipolysis and reduces adiposity, but results in elevated hepatic triglyceride and impaired insulin sensitivity. These results highlight the liver-adipose, Activin E-ALK7 signaling axis as a critical regulator of metabolic homeostasis.

© 2023 The Authors. Published by Elsevier GmbH. This is an open access article under the CC BY-NC-ND license (http://creativecommons.org/licenses/by-nc-nd/4.0/).

Keywords Adipose tissue; Lipolysis; Obesity; Diabetes

1. INTRODUCTION

Inter-organ communication or "crosstalk" allows for the coordination of energy metabolism across multiple organs to maintain metabolic homeostasis. The messengers of these inter-organ communication loops can include peptides, metabolites and, more recently, RNA packaged in exosomes [1]. As a key regulator of energy metabolism, the liver exchanges metabolic information with other organs by regulating circulating metabolites such as glucose, ketones, and triglyceride. In addition to these metabolite signals, the liver communicates to peripheral tissues by secreting peptides, termed "hepatokines". Hepatokine actions have been proposed in multiple metabolic organs including brain, adipose, pancreas, and muscle and dysregulation in these endocrine signaling networks has been linked to metabolic disease, but often without direct human genetic support [2]. Recently, human genome wide association studies (GWAS) report that predicted loss-of-function (pLOF) variants in the gene encoding the putative hepatokine Activin E, inhibin βE (*Inhbe),* associate with

Internal Medicine Research Unit, Pfizer Inc.,1 Portland Street, Cambridge, MA 02139, USA

*Corresponding author. E-mail: John.Griffin@Pfizer.com (J.D. Griffin).

Received October 10, 2023 • Accepted October 21, 2023 • Available online 28 October 2023

https://doi.org/10.1016/j.molmet.2023.101830

 © 2023 The Authors. Published by Elsevier GmbH. This is an open access article under the CC BY-NC-ND license (http://creativecommons.org/licenses/by-nc-nd/4.0/).

reduced visceral adiposity and improved indicators of metabolic function, including lower fasting glucose, lower serum triglycerides, and reduced incidence of diabetes [3,4]. Consistent with these data, elevations in hepatic *Inhbe* correlate with obesity and insulin resistance in mice, monkeys and humans [3,5,6]. These data implicate *Inhbe* and its associated hepatokine as potential regulators of body fat distribution and metabolic disease risk.

Inhbe is predominantly expressed in the liver where it encodes the monomeric inhibin βE subunit [7,8]. This subunit homo-dimerizes to form the secreted peptide Activin E, a member of the transforming growth factor-β (TGF-β) superfamily. The cells and organ systems targeted by Activin E, as well as the receptors through which Activin E signals, are not fully characterized. By extension, the physiological function of Activin E is undefined. *In vitro* experiments suggest that Activin E has both paracrine and endocrine functions, acting locally in hepatocytes to inhibit cell proliferation and as a hepatokine on adipocytes to increase expression of brown adipocyte markers [6,9,10]. *In vivo*, overexpression and knockdown of hepatic *Inhbe* both, paradoxically, reduce adipose tissue mass [5,6]. In total, these results support an endocrine function of Activin E on adipose tissue. However, the effect of Activin E on adipose function remains unclear.

In GWAS, pLOF variants in the Activin A Type 1 C gene (*Acvr1c)*, encoding the TGF-β receptor family member, ACVR1C or Activin Like Kinase 7 (ALK7), associate with similar metabolic traits to pLOF variants of *Inhbe*. These similarities suggest ALK7 as a possible receptor for Activin E [3,4,11]. While direct evidence of an Activin E-ALK7 ligand-receptor pair is lacking, this hypothesis is supported indirectly by experiments showing the effect of Activin E on adipocyte gene expression is neutralized by inhibition of activin type 1 receptors [6]. ALK7 is highly expressed in adipose tissue where it functions in regulation of lipolysis [12–14]. Upon ligand activation, ALK7 signals through the transcription factor SMAD2/3 to decrease the expression of lipolytic enzymes, although it is not clear whether this is the major or exclusive mechanism mediating its effect to reduce lipolysis [12]. While ALK7 has been suggested as a candidate receptor for Activin E, the influence of Activin E on adipose lipolysis has not been explored. In these studies, we demonstrate that Activin E is part of a liver-adipose communication loop. We find Activin E is positively regulated by increased hepatic fatty acid exposure secondary to increased adipose lipolysis. We show that Activin E acts as a hepatokine in adipose tissue, signaling through ALK7 to suppress lipolysis. Finally, we demonstrate that the Activin E-ALK7 signaling axis is a critical regulator of metabolic homeostasis, influencing adiposity and modulating the development of hepatic steatosis and insulin resistance during high fat diet feeding.

2. RESULTS

2.1. Hepatic *Inhbe* expression increases in response to elevated serum fatty acids

In mouse, rat, and human hepatocytes, insulin increases hepatic *Inhbe* expression [5,15]. Hepatic *Inhbe* is also elevated in models of obesity and insulin resistance [5]. While these observations suggest *Inhbe* may be positively regulated by insulin, in chow fed mice and rats *Inhbe* expression increases during fasting, a period characterized by low insulin [15–17]. To reconcile this apparent contradiction and gain insight into potential metabolic regulators of hepatic *Inhbe in vivo*, *Inhbe* expression was measured in livers of fed, fasted, and refed mice. After an overnight fast, hepatic *Inhbe* expression was significantly elevated compared to the ad-libitum fed state and this elevation was completely suppressed within 4 h of refeeding (Figure 1A). Plasma non-esterified free fatty acid (NEFA) and hepatic triglyceride (TAG) changed in parallel to hepatic *Inhbe* during fasting-refeed while glucose and insulin demonstrated an inverse response (Figure 1B–E). These observations suggested that increased fatty acid delivery to the liver, and the resulting increase in hepatic TAG, may act as a positive regulator of hepatic *Inhbe* expression. To test this hypothesis, chow fed mice were treated with CL 316,243, an agonist of the adipose tissue enriched β_3 receptor, to induce adipose lipolysis and increase fatty acid flux to the liver [18]. As expected, CL 316,243 significantly increased total plasma NEFA relative to untreated, fasted controls over 4 h following treatment (Figure 1F). Similarly, CL treatment resulted in a in a ~6 fold increase in hepatic TAG within 2 h following treatment and ~8 fold increase after 4 h (Figure 1G). Consistent with the hypothesis that increased hepatic TAG and/or increased circulating NEFA may positively regulate *Inhbe* expression, the elevated plasma NEFA and hepatic TAG resulting from CL treatment were associated with significant elevations in hepatic *Inhbe* transcript (Figure 1H).

The increase in circulating fatty acids during fasting and following CL 316,243 treatment is driven predominantly from increased liberation of FA from adipose tissue triglyceride. To determine if FA released from adipose can increase hepatic *Inhbe* expression, Huh7 human hepatocellular carcinoma cells were incubated with oleate and palmitate, the two most abundant fatty acids in human and mouse adipose tissue triglyceride [19,20]. As expected, incubation of Huh7 with both oleate and palmitate for 24hr resulted in a dose-dependent increase in expression of *CPT1α*, an established gene target of FA in hepatocytes, confirming Huh7 can respond transcriptionally to FA stimuli (Figure 1I–J) [21–24]. Similar to *CPT1α*, *Inhbe* expression also was increased dose-dependently following incubation with oleate and palmitate (Figure 1K-L). These observations are consistent with the hypothesis that FA released from hydrolysis of adipose triglyceride increase hepatocyte expression of *Inhbe*.

2.2. Loss of *Inhbe* increases fasting induced plasma NEFA and hepatic TAG accumulation

Although these data establish a relationship between increased hepatic *Inhbe* and elevations in plasma NEFA and hepatic TAG, the physiological consequences of increasing hepatic *Inhbe* during metabolic states associated with elevated plasma NEFA and hepatic TAG accumulation have not been established. To begin addressing this question, mice lacking expression of *Inhbe* in all tissues (INHBE KO) were challenged with an overnight fast and the physiological effects of *Inhbe* loss were ascertained. Genetic loss of *Inhbe* resulted in significantly elevated plasma NEFA levels during both 6 h and overnight fasting (Figure 2A). These sustained elevations in NEFA during prolonged fasting in mice lacking *Inhbe* correlated with significantly elevated hepatic TAG (Figure 2B). The effect of *Inhbe* knockdown on fasting plasma NEFA and hepatic TAG was consistent between male and female mice (Figure 2C–D). Loss of *Inhbe* in male mice did not alter fasting blood glucose but increased serum insulin levels after an overnight fast (Figure 2E–F). Genetic loss of *Inhbe* did not affect fasting glucose or insulin levels in female mice (Figure 2G–H).

2.3. Activin E suppresses adipose lipolysis

Elevated circulating NEFA in INHBE KO mice suggests that Activin E may influence fatty acid release from adipose, fatty acid uptake and metabolism, or both. To begin assessing the role of Activin E on adipocyte lipolysis several adipocyte cell lines were screened for (1) the expression of the type 1 and type 2 activin receptors necessary to mediate activin ligand signaling as well as (2) their ability to increase SMAD phosphorylation following treatment with activin type 1 receptor

 © 2023 The Authors. Published by Elsevier GmbH. This is an open access article under the CC BY-NC-ND license (http://creativecommons.org/licenses/by-nc-nd/4.0/).

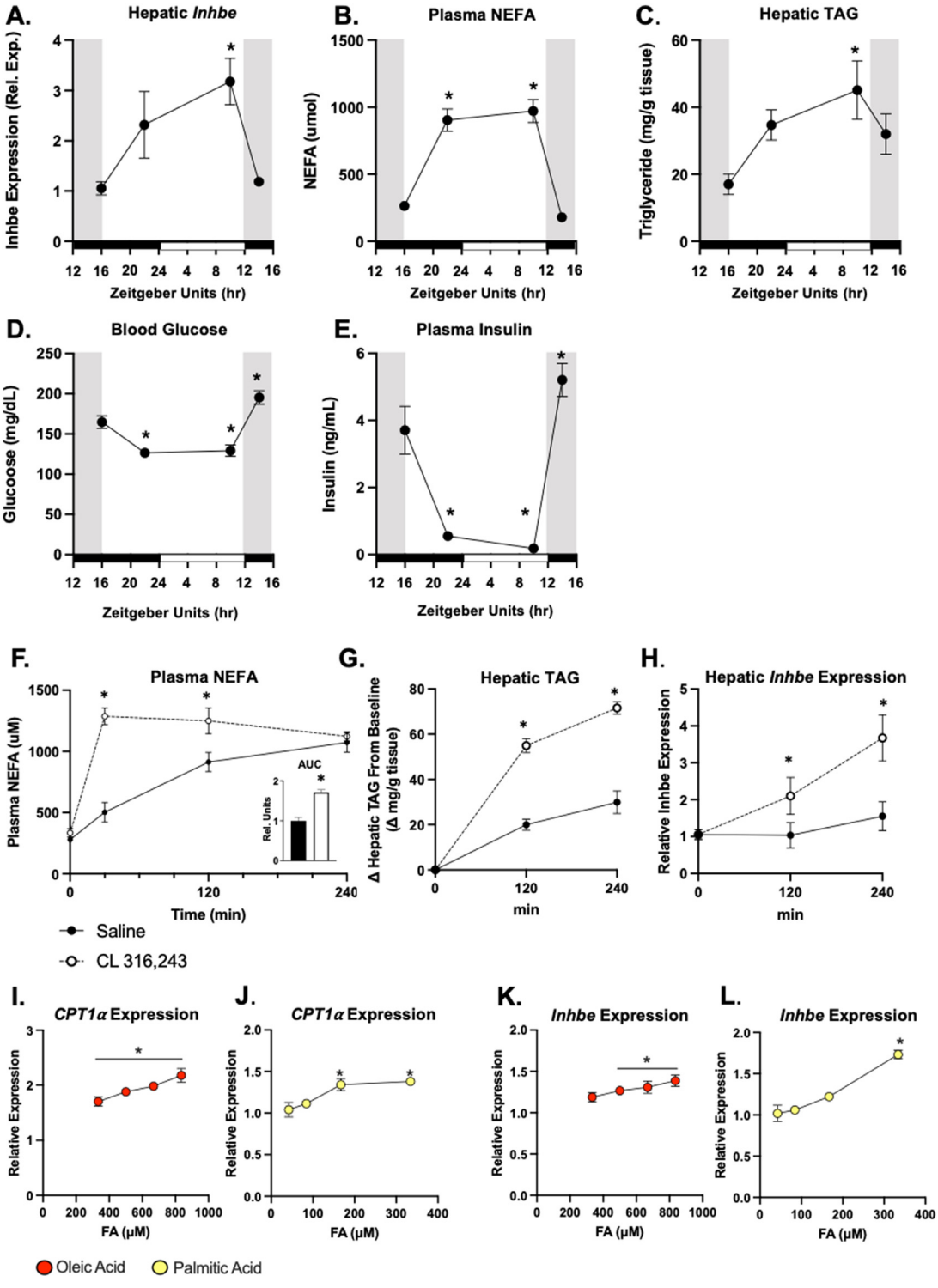

Figure 1: Hepatic *Inhbe* Expression Is Increased by Free Fatty Acids. (A) Hepatic *Inhbe* gene expression, **(B)** plasma non-esterified fatty acids (NEFA), **(C)** hepatic triglyceride (TAG), **(D)** tail vein glucose and **(E)** plasma insulin from 10 to 12 weeks old, male C57BL6 mice collected under ad-libitum fed, 6hr fasting, 18hr fasting, or 4hr refed conditions. Gray zones on graph represent periods of ad-libitum feeding. White zones represent periods of fasting. Black and white horizontal bars represent dark and light cycle, respectively. Data are presented as mean ± S.E.M. n = 9 mice/timepoint. * = $p \leq 0.05$ via Student's t-test compared to fed-state. **(F)** Plasma NEFA, **(G)** hepatic TAG, and **(H)** hepatic *Inhbe* gene expression in 16–20 week old mice injected intraperitoneally with 100ug/kg CL 316,243 or saline in the fed state. Following injection food was removed, tail vein blood was collected at indicated time points and mice were euthanized after 120 or 240 min. For g & h, "baseline" data used for normalization was collected from mean of an untreated control group euthanized at time of injection. Data are presented as mean ± S.E.M. n = 8–14 mice/grp/timepoint * = $p \leq 0.05$ via Student's t-test CL 316,243 vs saline within each timepoint. **(I–L)** Expression of *CPT1α* and *Inhbe* in Huh7 hepatocellular carcinoma cells treated with indicated concentrations of fatty acids for 24hrs. Expression normalized to the geometric mean of *Ppia, Ppib,* and *Gapdh* and expressed relative to untreated cells incubated in 1 % BSA control media. Data are presented as mean ± S.E.M. n = 3–4 wells/dose * = $p \leq 0.05$ via Student's t-test vs. untreated controls within each dose group.

 © 2023 The Authors. Published by Elsevier GmbH. This is an open access article under the CC BY-NC-ND license (http://creativecommons.org/licenses/by-nc-nd/4.0/).

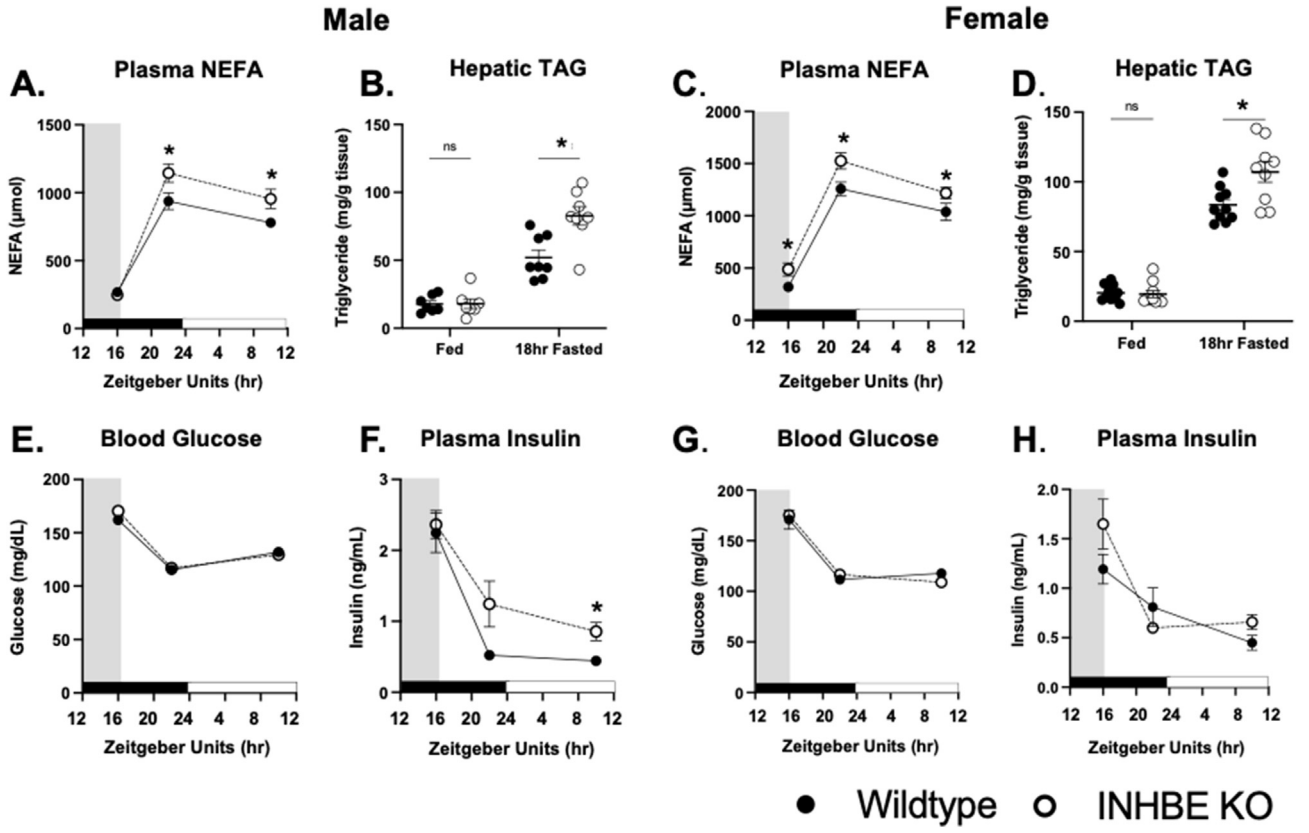

Figure 2: Loss of *Inhbe* Increases Fasting NEFA & Hepatic TAG. (A—D) Plasma non-esterified fatty acid (NEFA) and hepatic triglyceride (TAG) from 10 to 12 weeks old, chow fed (A,C) male and (B,D) female *Inhbe* knockout mice collected under ad-libitum fed, 6 h fasting, or 18hr fasting conditions. **(E—H)** Blood glucose and plasma insulin from 10 to 12 week old, chow fed (E,G) male and (F,H) female *Inhbe* knockout mice collected under ad-libitum fed, 6hr fasting, or 18hr fasting conditions. Gray zones on graph represent periods of ad-libitum feeding. White zones represent periods of fasting. Black and white horizontal bars represent dark and light cycle, respectively. All experiments performed at room temperature. Data are presented as mean ± S.E.M. n = 15 mice/timepoint * = $p \leq 0.05$ via Student's t-test compared to fed-state.

ligands. All activin receptors were expressed in immortalized mouse brown adipocytes (mBAds) (Figs. S1A—E). In contrast, 3T3-L1 adipocytes expressed *Acvr1c*, the gene encoding the ALK7 receptor at low levels. In line with these expression data, mBAD increased SMAD phosphorylation in response to known ALK7 ligands, while 3T3L1 adipocytes did not (Figs. S1F—G). Given the absence of ALK7 responsiveness in 3T3L1, mBAds were further pursued as an activin-responsive model adipocyte system for these studies. To confirm the ability of mBAD cells to suppress lipolysis in response to activin ligands, adipocytes were treated with Activin B, which signals through ALK4 and ALK7, and Activin C, which signals through ALK7, for 24hr and then stimulated with isoproterenol. Both Activin B and Activin C elicited a concentration-dependent suppression of NEFA release, substantiating mBAd cells as an appropriate model system to study activin regulation of lipolysis *in vitro* (Figure 3A).

Understanding the effect of Activin E on adipocyte lipolysis is complicated by a lack of available purified Activin E. To overcome this obstacle, an INHBE conditioned media (CM) was prepared by transfecting the Expi293F embryonic kidney cell line with a plasmid encoding mouse or human INHBE (mINHBE and hINHBE, respectively) and harvesting culture media enriched with INHBE 96 h after transfection. A control conditioned media was also generated by stable transfection with an empty-vector plasmid. Incubation of mBAds with INHBE conditioned media for 24hr led to a concentration-dependent suppression of isoproterenol-stimulated NEFA release (Figure 3B). Treatment of mBAds with both mouse and human INHBE CM at a 3 % final concentration resulted in ~50 % suppression of NEFA release. Empty vector control conditioned media (EVCM) had no effect on isoproterenol stimulated NEFA release, indicating that the suppressive effect INHBE CM on NEFA release was not due to non-specific effects of the CM. To confirm that the lipolytic suppression observed with CM treatment of mBAds was a result of Activin E in the media, lipolysis experiments were repeated with CM that had been immunologically depleted of Activin E. Immunoadsorption of mINHBE CM reduced mouse INHBE peptide by over 40 % relative to IgG controls (Fig. S2A), but did not diminish INHBE peptide in hINHBE CM, suggesting the Activin E antibody did not recognize human Activin E. Depletion of Activin E from mINHBE CM significantly blunted lipolytic suppression to a degree comparable to the reduction in INHBE peptide (Fig. S2B). As expected, anti-Activin E immunoadsorption of hINHBE CM did not affect mBAd lipolysis compared to depletion by IgG control hINHBE CM, consistent with ineffective immunoadsorption of human Activin E by the Activin E antibody. Activin E pulldown of EVCM and Activin B containing media did not affect mBAd lipolysis relative to within group IgG depletion controls, indicating that the Activin E pulldown procedure depleted Activin E peptide specifically. In sum, these data show that the lipolytic suppression by INHBE CM in mBAds was due specifically to the presence of bioactive Activin E in the CM. To understand better the mechanisms by which Activin E reduces adipocyte lipolysis, the suppressive effect of INHBE CM on stimulated lipolysis was determined

 © 2023 The Authors. Published by Elsevier GmbH. This is an open access article under the CC BY-NC-ND license (http://creativecommons.org/licenses/by-nc-nd/4.0/).

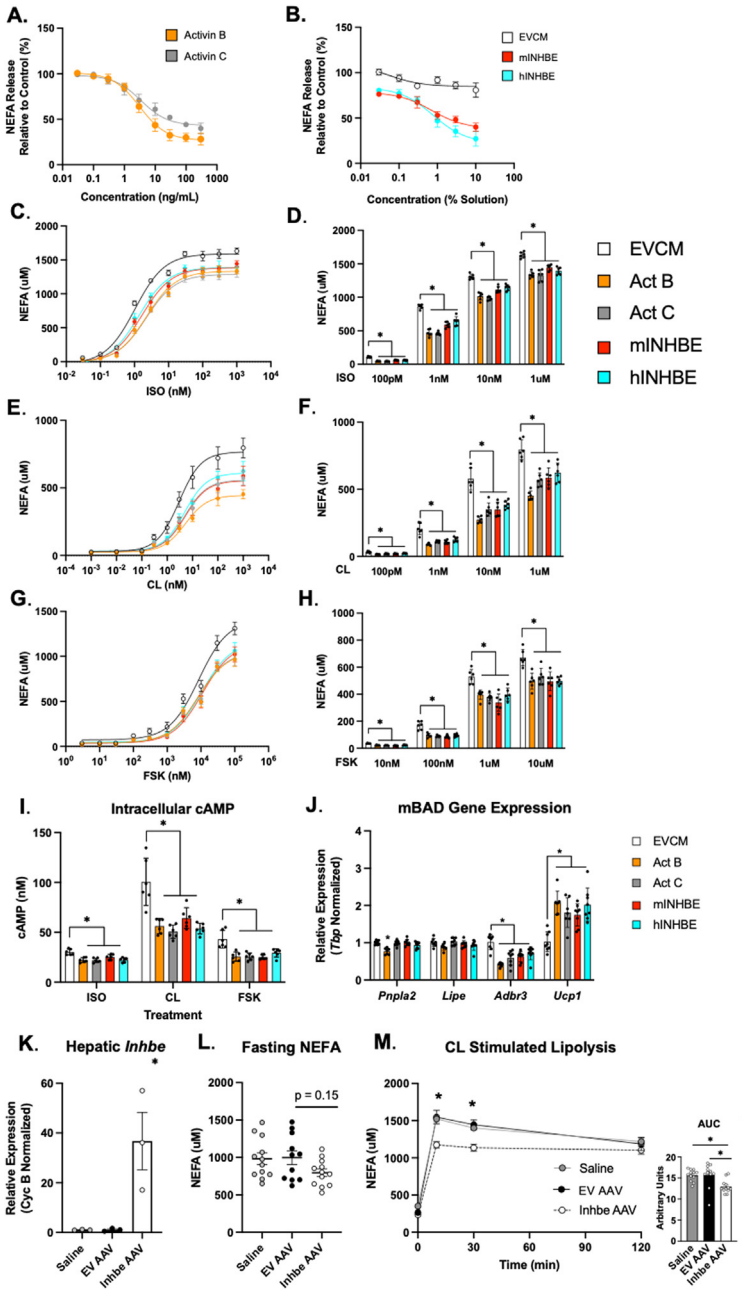

Figure 3: Activin E Conditioned Media Suppresses Adipocyte Free Fatty Acid Release. (A—B) Non-esterified fatty acid (NEFA) release from differentiated immortalized mouse brown preadipocytes treated for 24hrs with no ligand (Krebs Ringer HEPES Buffer, KRBH), Activin B in KRBH, Activin C in KRBH, or indicated concentrations of conditioned media (CM) enriched with mouse or human INHBE (mINHBE and hINHBE, respectively) on day 7 post-differentiation. Media harvested from empty vector transfected cells (EVCM) was used as a control treatment. Following incubation, cells were treated with 1 nm isoproterenol. At the end of 2hr media was collected for analysis. Data points represent mean ± S.E.M. of 3—4 experimental replicates. All data normalized to untreated, control cells. **(C—H)** Representative dose—response of NEFA release from differentiated immortalized mouse brown preadipocytes incubated as above with 3 % solutions of CM. Following incubation cells were treated with indicated doses of (C—D) isoproterenol, (E—F) CL 316,243, or (G—H) forskolin. Data are presented as mean ± S.E.M. Data points represent individual wells. n = 3—6 wells/dose. * = $p \leq 0.05$ via one-way ANOVA within each dose **(I)** Intracellular cyclic AMP concentrations in differentiated mBAD treated with 1 nm isoproterenol, 1 nm CL316,243, or 1 μM forskolin. Data are presented as mean ± S.E.M. Data points represent individual wells. n = 5—6 wells/dose. * = $p \leq 0.05$ via one-way ANOVA. **(J)** Gene expression of lipolytic target genes from immortalized mouse brown preadipocytes treated with 3 % solutions of conditioned media for 24hrs. Data are presented as mean ± S.E.M. Data points represent individual wells. n = 6—8 wells/grp. * = $p \leq 0.05$ via one-way ANOVA within each gene. **(K)** Hepatic expression of *Inhbe* in fed mice 4 weeks following treatment with $3*10^{11}$ g.c. AAV8-TBG adenovirus expressing empty vector (EV AAV) or the coding region of mouse *Inhbe* (Inhbe AAV). A saline treated group was used as an additional control. Data are presented as mean ± S.E.M. Data points represent individual mice. n = 3 mice/grp * = $p \leq 0.05$ via one-way ANOVA. **(L)** Plasma NEFA in mice fasted for 6hrs. Data collected 8 weeks following treatment with indicated adenovirus. Data are presented as mean ± S.E.M. Data points represent individual mice. n = 10—12/grp * = $p \leq 0.05$ via one-way ANOVA. **(M)** Plasma NEFA at indicated timepoints and area under the curve (AUC) from mice injected with 100ug/kg CL316,243 12 weeks following treatment with indicated adenovirus or saline. Experiment performed at room temperature. Data are presented as mean ± S.E.M. For AUC, data points represent individual mice. n = 12 mice/grp * = $p \leq 0.05$ via one-way ANOVA. (For interpretation of the references to color in this figure legend, the reader is referred to the Web version of this article.)

 © 2023 The Authors. Published by Elsevier GmbH. This is an open access article under the CC BY-NC-ND license (http://creativecommons.org/licenses/by-nc-nd/4.0/).

using three different lipolytic agonists: (1) isoproterenol, a non-selective β-adrenergic receptor agonist, (2) CL 316,243 a β_3 specific receptor agonist, and (3) forskolin, which activates adenylate cyclase in a receptor-independent manner. Compared to adipocytes treated with EVCM, both mouse and human INHBE CM treatment blunted submaximal and maximal stimulated NEFA release across all three lipolytic activators. (Figure 3C—H). The suppressive effect of INHBE CM treatment on adipocyte NEFA release was similar to the effects of the two ALK7 ligands, Activin B and Activin C. In addition to suppressing adipocyte NEFA release, treatment of mouse brown adipocytes with Activin E also significantly reduced intracellular cAMP, a mediator of adipocyte lipolysis, following stimulation with the three lipolytic agonists (Figure 3I). In total, these data are consistent a role for Activin E in suppression of adipocyte lipolysis.

To gain further insight into the mechanisms by which Activin E suppresses adipocyte NEFA release, the expression of several genes related to adipocyte NEFA metabolism were measured. The expression of the β_3 adrenergic receptor, *Adrb3*, was reduced, while the expression of *Ucp1*, an uncoupler of cellular respiration, was increased following mouse and human INHBE conditioned media treatment (Figure 3J). These changes were consistent in mBAds treated with Activin B and Activin C. The expression of canonical lipases, *Pnpla2* and *Lipe*, were not affected by 24hr INHBE CM treatment.

To determine if elevated hepatic Activin E could suppress lipolysis *in vivo, Inhbe* was overexpressed in mice using an AAV8 adenoviral construct encoding mouse *Inhbe* under the control of the hepatocyte specific thyroxine binding globulin (TBG) promoter (Inhbe AAV) and stimulated NEFA levels were determined (Fig. S3A) [25]. Four weeks after infection with Inhbe AAV, hepatic expression of *Inhbe* mRNA was increased ∼40-fold relative to mice infected with empty vector AAV (EV AAV) or treated with saline (Figure 3K). The hepatic *Inhbe* transcript levels achieved following Inhbe AAV treatment were 20 fold greater than *Inhbe* expression observed in overnight fasted mice and 8 fold greater than *Inhbe* transcript levels in mice a high fat diet for 12 weeks (Fig. S3B). No increase in *Inhbe* expression was observed in adipose tissue of Inhbe AAV treated mice relative to both EV AAV and saline treated controls, confirming liver-specific overexpression (Fig. S3C). Consistent with an effect of Activin E on lipolysis, liver specific overexpression of *Inhbe* reduced fasting circulating NEFA by over 20 % relative to EV AAV treated controls, although this difference failed to reach statistical significance (Figure 3L). In addition, Inhbe AAV treated mice demonstrated a significant reduction in peak and total NEFA release following stimulation of lipolysis by CL 316, 243 compared to EV AAV and saline treated controls (Figure 3M). In total, these data support the hypothesis that Activin E produced by the liver acts as a negative regulator of adipose lipolysis.

2.4. Activin E signals through ALK7 to suppress lipolysis

Although the receptor for Activin E has not been identified, the similarities in phenotype for loss-of-function human polymorphisms in the Activin A Type 1C receptor gene, *Acvr1c*, encoding the receptor ACVR1C or ALK7, and *Inhbe* suggest that ALK7 may be the physiological receptor for Activin E [3,4,11,26]. To determine the receptor through which Activin E signals, HEK293T cells, which do not express detectable levels of endogenous ALK7, were transfected with constructs coding for ALK7 as well as the activin co-receptor, Cripto, which facilitates activin ligand-receptor binding [27]. Transfected cells were treated with conditioned media enriched for INHBE and SMAD signaling was quantified by western blotting for SMAD2/3 phosphorylation (Figure 4A). Treatment with control EVCM produced a small, but significant ∼1.7× increase in SMAD2 phosphorylation in ALK7 transfected groups relative to empty vector controls that was blocked by the activin type 1 receptor antagonist, SB 431542, likely indicating the presence of residual activins secreted from cells producing conditioned media (Figure 4B). Activin B elicited a ∼7× increase in SMAD phosphorylation in all transfected cells, confirming the presence of ALK4 as well as the Activin Type 2 receptors necessary for Activin-SMAD signaling in this cell model (Figure 4C). Both mouse and human INHBE conditioned media increased SMAD phosphorylation only in cells that had been transfected with plasmids expressing ALK7 (Figure 4D—E). Further, this ALK7 dependent SMAD phosphorylation was completely suppressed by treatment with SB 431542. CM treatment produced increases in SMAD3 phosphorylation that were indistinguishable from increases in SMAD2 (Figs. S4A—D). These findings were confirmed using the HEK293SBE SMAD reporter line (Figs. S5A—D). In sum, these results suggest that ALK7 is necessary for Activin E mediated SMAD phosphorylation and is a candidate physiological receptor for Activin E.

To validate that the SMAD signaling response was due specifically to Activin E in CM, Activin E from mouse and human CM was depleted by immunoadsorption prior to treatment of HEK293SBE cells. SMAD signaling induced by mINHBE CM was reduced by over 60 % following Activin E depletion relative to IgG pulldown (Fig. S5E). SMAD signaling in response to hINHBE CM treatment was reduced by Activin E depletion by 6 %, likely reflecting the ineffectiveness of the Activin E antibody to bind human Activin E in CM. EVCM and Activin B mediated SMAD signaling was not affected by Activin E pulldown, confirming the specificity of Activin E depletion under these pulldown conditions. In sum, depletion experiments strongly suggest that the SMAD signaling in response to INHBE CM treatment was due specifically to Activin E in the media.

To explore whether ALK7 is required for Activin E signaling in adipocytes, CRISPR-Cas9 was used to disrupt ALK7 exons 4 or 5, which encode the receptor's kinase domain, in mBAds and then SMAD phosphorylation following treatment with activins or conditioned media was determined. Targeting either exon 4 or 5 reduced ALK7 transcript by roughly 50 % in fully differentiated adipocytes without affecting expression of other activin type 1 receptors (Fig. S6A). ALK7 gene editing did not affect adipocyte differentiation or basal or isoproterenol-stimulated lipolysis (Figs. S6B—D). Treatment of mBADs with ALK7 ligands Activin C and GDF3 robustly increased SMAD2 phosphorylation in naïve and Rosa26 edited cells, but failed to stimulate SMAD2 phosphorylation in ALK7 edited cells, confirming loss of functional ALK7 with CRISPR (Figure 4F). mINHBE and hINHBE CM treatment of ALK7 edited mBADs failed to stimulate SMAD phosphorylation, indicating ALK7 is required for Activin E mediated SMAD signaling in adipocytes. In support of this result, mINHBE CM increased SMAD2 phosphorylation in primary adipocytes isolated from wildtype mice, but not in adipocytes isolated from ALK7 kinase deficient mice (Fig. S7).

Next, the CRISPR-edited ALK7 brown adipocyte model was employed to determine if ALK7 is required for Activin E suppression of adipocyte lipolysis. In cells treated with the ALK4 and ALK7 ligand, Activin B, disruption of ALK7 slightly blunted Activin B mediated lipolytic suppression, indicated by a small, but significant increase in NEFA release relative to naïve and Rosa26 edited cells (Figure 4G). In contrast to Activin B, suppression of lipolysis by the ALK7 specific ligand, Activin C, was completely blocked by ALK7 targeting, providing additional confirmation that the targeting strategy successfully interrupted ALK7 signaling. The suppressive effects of INHBE conditioned media on adipocyte NEFA release were almost completely blocked by ALK7 targeting.

To determine the physiological relevance of the ALK7 signaling axis on the regulation of lipolysis *in vivo*, fasting and CL-stimulated NEFA were

 © 2023 The Authors. Published by Elsevier GmbH. This is an open access article under the CC BY-NC-ND license (http://creativecommons.org/licenses/by-nc-nd/4.0/).

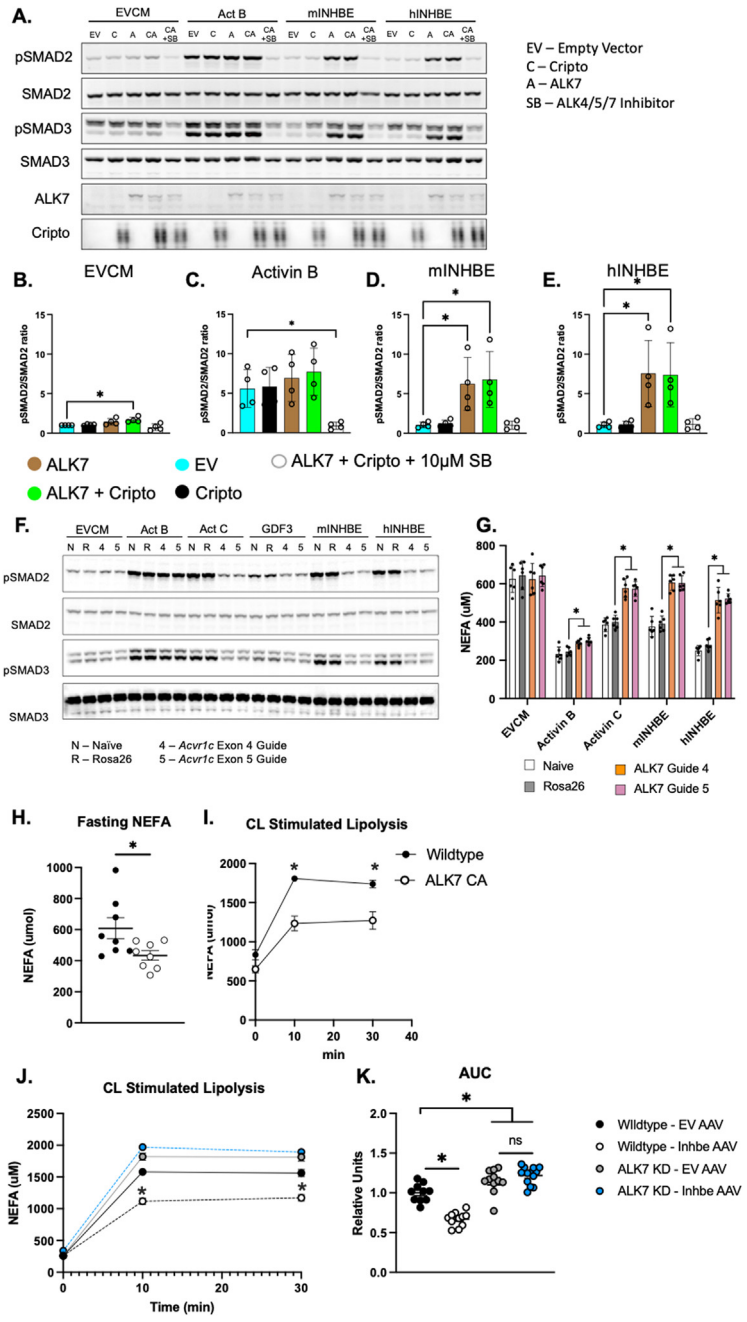

Figure 4: Activin E Signals Through ALK7 To Suppress Adipose Lipolysis. (A) Representative western blot of SMAD phosphorylation in HEK293T transfected with indicated constructs, treated with empty vector conditioned media (EVCM), EVCM plus 25 ng/mL Activin B, or CM enriched with mouse or human INHBE (mINHBE and hINHBE, respectively) for 30mins. Where indicated, cells were pretreated for 30 min with SB-431542 prior to ligand addition. **(B–E)** Densitometric quantitation of pSMAD2:Total SMAD2 for cells treated with indicated ligands. Data are normalized to mean of empty vector transfected cells treated with EVCM and presented as mean ± S.E.M. of 4 experimental replicates. Data points represent values from independent experiments. * = $p \leq 0.05$ analyzed by one-way ANOVA **(F)** Representative western blot of SMAD phosphorylation in differentiated immortalized mouse brown preadipocytes following CRISPR mediated gene editing using indicated guides. **(G)** Non-esterified fatty acid (NEFA) release from differentiated immortalized mouse brown preadipocytes following CRISPR mediated gene editing. Cells were treated for 24hrs with indicated ligands prior to starvation and stimulation with 1 nm isoproterenol. Data are presented as mean ± S.E.M. Data points represent individual wells. n = 4–6 wells/grp. * = $p \leq 0.05$ analyzed by one-way ANOVA. Data are representative of two independent experiments. **(H)** Plasma NEFA in 12 week old, chow fed male ALK7 constitutively active (ALK7 CA) mice fasted for 6hr. Data are presented as mean ± S.E.M. Data points represent indivudal mice. n = 8 mice/grp. * = $p \leq 0.05$ analyzed by Student's t-test. **(I)** Plasma NEFA in 16 week old, chow fed male mice injected intraperitoneally with 100ug/kg CL 316,243 in the fed state. Following injection food was removed and tail vein blood was collected at indicated time points. Data are presented as mean ± S.E.M. n = 8 mice/grp/timepoint. * = $p \leq 0.05$ analyzed by Student's t-test within each timepoint. **(J–K)** (J) Plasma NEFA and (K) baseline normalized area under the curve (AUC) in mice treated with an AAV8-TBG encoding mouse *Inhbe* (Inhbe AAV) or an empty vector (EV AAV) control. 10 weeks following AAV treatment mice were injected intraperitoneally with 100ug/kg CL 316,243 in the fed state. Following injection food was removed and tail vein blood was collected at indicated time points. Data are presented as mean ± S.E.M. n = 10–12 mice/grp/timepoint * = $p \leq 0.05$, Wildtype – EV vs. Wildtype - Inhbe via one-way ANOVA and Tukey's HSD posthoc testing within each timepoint. (For interpretation of the references to color in this figure legend, the reader is referred to the Web version of this article.)

 © 2023 The Authors. Published by Elsevier GmbH. This is an open access article under the CC BY-NC-ND license (http://creativecommons.org/licenses/by-nc-nd/4.0/).

measured in mice harboring a mutation in the ALK7 kinase domain rendering the receptor's kinase function constitutively active (ALK7 CA) [12]. Both fasting and CL-stimulated plasma NEFA were significantly reduced in ALK7 CA mice compared to wildtype controls (Figure 4H—I). These *in vivo* results agree with *in vitro* data indicating activation of ALK7 suppresses adipose NEFA release.

To determine if Activin E requires ALK7 to suppress lipolysis *in vivo*, wildtype mice and mice harboring a loss-of-function mutation in the ALK7 kinase domain (ALK7 KD) were treated with Inhbe AAV and NEFA release following CL-stimulation was measured. Within EV treated groups, ALK7 kinase deficiency alone increased CL-stimulated NEFA release relative to wildtype mice, in line with previous reports demonstrating ALK7 LOF increases lipolysis [12,13]. Treatment of wildtype mice with Inhbe AAV suppressed CL stimulated NEFA release ~35 % compared to wildtype mice treated with control EV AAV (Figure 4J—K). In contrast, Inhbe AAV treatment failed to reduce CL-stimulated NEFA release in ALK7 KD mice, indicating that kinase-competent ALK7 is required for Inhbe AAV mediated suppression of lipolysis *in vivo*.

In total, the combined results of signaling experiments, as well as *in vitro* and *in vivo* lipolysis studies, suggest that hepatic Activin E signals through ALK7 in adipocytes to suppress lipolysis.

2.5. Genetic knockdown of *Inhbe* results in elevated hepatic TAG and reduced insulin sensitivity

Mice with global ablation of *Inhbe* show no metabolic phenotype when housed at ambient temperature (22 °C, Tα) [14]. However, Tα represents a thermal stress for mice which may confound interpretation of metabolic phenotyping results [28]. To determine the metabolic consequences of *Inhbe* loss-of-function at murine thermoneutral conditions, (30 °C, Tn), and isolate for any confounding effects of thermal stress, *Inhbe* germline knockout mice were generated and their metabolic phenotype characterized during chow and HFD feeding under Tn. Genetic deletion of *Inhbe* significantly reduced body weight during HFD feeding, but not when mice were fed chow (Figure 5A). Average weekly food intake was not different between groups throughout both chow and HFD feeding (Fig. S8). MRI quantification of body composition revealed significant reductions in adiposity and increased relative lean mass in HFD fed INHBE KO mice relative to HFD fed controls (Figure 5B—C). Adiposity was numerically reduced in chow fed INHBE KO mice, although this difference failed to reach statistical significance (18.1 % Chow - WT vs 14.6 % Chow - INHBE KO, $p = 0.163$). Despite reduced adiposity, both liver weight and TAG content were significantly elevated in HFD fed INHBE KO mice (Figure 5D—E). In contrast to mice housed at Tα (Figure 2A—H), chow fed INHBE KO mice showed no differences in fasting plasma NEFA at thermoneutrality (Figure 5F). Plasma NEFA was significantly increased in INHBE KO mice within 3 weeks of initiating HFD feeding (Figure 5F). To determine the impact of *Inhbe* loss on glucose-insulin homeostasis fasting glucose and insulin were measured. INHBE KO mice displayed a trend toward elevated fasting glucose on chow and HFD diet (Figure 5G). Fasting insulin was significantly elevated in INHBE KO mice fed HFD, indicative of insulin resistance (Figure 5H). Consistent with these results, the homeostatic model assessment of insulin resistance (HOMA-IR), a surrogate measure of insulin resistance, was significantly elevated in INHBE KO mice fed HFD (Figure 5I). To further assess glucose-insulin metabolism following loss of *Inhbe*, INHBE KO mice were challenged with an insulin tolerance test (ITT). The glucose-suppressive effects of insulin were significantly blunted in both chow and HFD fed INHBE KO mice as evident by significantly elevated glucose AUC during the ITT (Figure 5J—K). A significant elevation in glucose AUC during ITT was also observed when baseline glucose was controlled for (Fig. S9). In total, these data show that in spite of protection from increased adiposity, loss of *Inhbe* results in insulin resistance.

3. DISCUSSION

In this study we identify an inter-organ feedback loop involving regulation adipose tissue lipolysis by the hepatokine, Activin E. We find that hepatic expression of Activin E is positively correlated with increased liver NEFA exposure both *in vivo* and *in vitro*. In addition, we demonstrate that ablation of Activin E in mice leads to elevated fasting plasma NEFA and hepatic TAG, suggesting that liver-secreted Activin E influences metabolic processes controlling circulating NEFA. Taken together, these data are consistent with a regulatory model in which Activin E is secreted from liver in response to elevated circulating NEFA and functions as a hepatokine to suppress adipose lipolysis. In support of this hypothesis, we demonstrate that Activin E suppresses NEFA release in cultured adipocytes and in fasted and CL 316,243 treated mice. We show that the suppression of adipose NEFA release by Activin E requires the adipose enriched activin receptor, ALK7. Finally, using a mouse model of *Inhbe* knock out, we demonstrate that disruption of the Activin E-ALK7 signaling axis leads to increased hepatic TAG accumulation and insulin resistance during HFD feeding. In total, these data support a role for Activin E in mediating liver-adipose, inter-organ communication and indicate that this signaling axis is essential for maintaining metabolic homeostasis. Hepatokines are dynamically regulated in response to metabolic stimuli including exercise, fasting, inflammation and insulin resistance [2,29,30]. In line with its role as a hepatokine, hepatic *Inhbe* also exhibits metabolic regulation, increasing in mice during chronic HFD feeding, in mice and rats during fasting, following CL 316,243 treatment in mice, and in hepatocytes treated with insulin [6,15—17,31]. However, the precise metabolic stimuli regulating *Inhbe* have not been identified. In this study, hepatic *Inhbe* expression was found to be increased in mice during fasting and following CL 316,243 treatment, two metabolic challenges that result in significant increases in circulating NEFA and hepatic TAG, implicating these metabolites as possible regulators of hepatic *Inhbe* expression.

To date, insulin has been considered the primary, positive regulator of hepatic *Inhbe* expression. This is based on an increase in *Inhbe* expression following insulin treatment of cultured hepatocytes and human observational data in which hepatic *Inhbe* expression correlated with indicators of insulin resistance [5,15]. In the present study, a positive correlation between hepatic *Inhbe* expression and circulating insulin was not observed during fast-refeeding studies. On the contrary, *Inhbe* expression was found to be higher during low-insulin, fasted states than high-insulin, fed and ad-libitum fed states. Thus, acute elevations in insulin from feeding are not associated with elevated hepatic *Inhbe in vivo*, arguing against insulin as a direct regulator of *Inhbe* expression. It is therefore possible that the association between high insulin and elevated hepatic *Inhbe* seen in humans with metabolic disease is related to a secondary consequence of chronically high insulin, rather than a direct effect of high insulin itself.

Two metabolic consequences common to all conditions associated with increased hepatic *Inhbe*, including fasting, accelerated lipolysis, and insulin resistance, are elevated hepatic TAG and increased circulating NEFA, suggesting that liver TAG and/or circulating NEFA may be a primary regulator of hepatic *Inhbe*. A TAG/NEFA-centric model for hepatic *Inhbe* regulation has several important

 © 2023 The Authors. Published by Elsevier GmbH. This is an open access article under the CC BY-NC-ND license (http://creativecommons.org/licenses/by-nc-nd/4.0/).

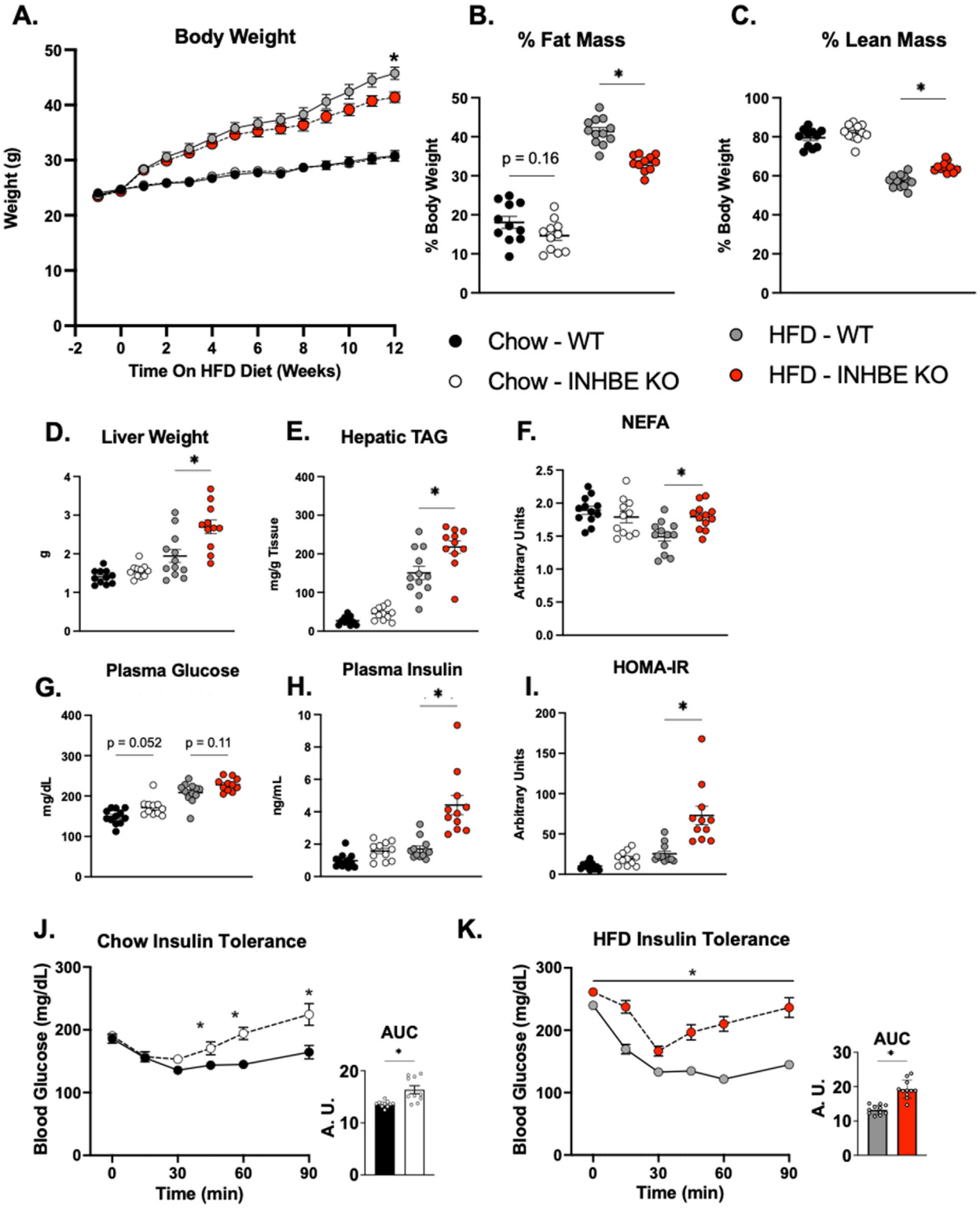

Figure 5: Knockout of INHBE Protects from HFD Induced Obesity, but Increases Hepatic TAG and Impairs Insulin Sensitivity (A) Body weight of male wildtype (WT) and Inhbe knockout (INHBE KO) mice fed chow and 60 % high fat diet (HFD) for 12 weeks. **(B)** Relative fat mass and **(C)** relative lean mass after 11 weeks of diet treatment. **(D–E)** Liver weight and hepatic triglyceride content of wildtype and INHBE KO after 12 weeks of chow or HFD feeding. **(F)** 6hr fasting plasma non-esterified fatty acids (NEFA) after 3 weeks of chow or HFD feeding. **(G–H)** 6hr fasting blood glucose and plasma insulin measured from tail nick and submandibular bleed, respectively, following 9 weeks of HFD. **(I)** Homeostatic model assessment of insulin resistance (HOMA-IR) calculated from blood glucose and plasma insulin collected after 9 weeks of diet treatment. Data are presented as mean ± S.E.M. n = 11–12/grp. * = $p \leq 0.05$ via Two-way ANOVA and Tukey's HSD posthoc testing. **(J–K)** Blood glucose excursions following intraperitoneal injection of insulin in mice fed (J) chow or (K) HFD for 4 weeks. Area under the curve (AUC) of blood glucose over time is shown adjacent to each graph. All experiments performed at thermoneutrality Data are presented as mean ± S.E.M. Where shown, data points represent values from individual mice. n = 11–12/grp. * = $p \leq 0.05$ via Student's t-test at each timepoint.

 © 2023 The Authors. Published by Elsevier GmbH. This is an open access article under the CC BY-NC-ND license (http://creativecommons.org/licenses/by-nc-nd/4.0/).

implications. First, it supports the hypothesis that elevated hepatic *Inhbe* observed in individuals with insulin resistance is not a direct effect of insulin signaling. Under this model, increased hepatic Activin E in the insulin resistant state is a consequence of elevated hepatic TAG or the increase in adipose lipolysis associated with metabolic disease. This, by extension, implies that elevated Activin E is not causative of insulin resistance. Second, direct regulation of hepatic *Inhbe* by hepatic TAG or NEFA suggests a possible physiological role for Activin E: reciprocal control of hepatic TAG. By this model, increased hepatic TAG results in an increase in circulating Activin E which then serves as "brake", acting as an endocrine factor to suppress lipolysis, reduce NEFA efflux from adipose tissue, and ultimately reduce hepatic TAG accumulation.

While the consistent associations between hepatic *Inhbe*, hepatic TAG and circulating NEFA observed in these experiments supports a TAG/NEFA-centric regulatory model for *Inhbe* expression, the transcriptional regulation of Activin E has not been fully elucidated. Interestingly, hepatocyte specific knockdown of PPARα in mice prevented upregulation of hepatic *Inhbe* during fasting and following CL 316,243 treatment. As endogenous fatty acids act as PPARα ligands, these data in combination with present results suggest that fatty acids released from adipose tissue lipolysis may increase hepatic *Inhbe* by activating PPARα. However, additional concurrent metabolic changes other than hepatic TAG/NEFA remain candidates as proximal regulators of *Inhbe* expression.

Supporting the hypothesis that Activin E acts in a feedback loop to regulate hepatic TAG levels, knockdown of *Inhbe* increased hepatic TAG during fasting and HFD feeding. The increase in hepatic TAG following *Inhbe* knockout occurred alongside significant elevations in circulating NEFA, which positively contribute to hepatic TAG balance, suggesting that *Inhbe* may influence hepatic TAG levels via modulation of circulating NEFA [32]. While net circulating NEFA during fasting is the sum of multiple metabolic processes, the majority of NEFA in circulation during fasting is derived from adipose tissue lipolysis [33]. These data are consistent with a model wherein Activin E modulates adipose tissue NEFA release to regulate hepatic TAG. In support of this model, treatment of mouse adipocytes with Activin E conditioned media antagonized lipolysis and overexpression of *Inhbe* in mice reduced CL 316,243 stimulated NEFA release. Interestingly, other hepatokines have also been shown to regulate hepatic TAG through their actions on adipose tissue NEFA release suggesting that the liver-adipose signaling axis has redundant mechanisms for endocrine control of hepatic TAG levels [29].

The link between Activin E and adipose tissue metabolism is supported by recent human GWAS which identified an association between *Inhbe* predicted loss-of-function gene variants and reduced visceral adiposity [3,4]. Interestingly, loss-of-function genetic variants in the adipose enriched activin receptor ALK7, were similarly associated with reduced visceral adiposity [3,4,11,26]. This similarity in phenotypes between ALK7 and *Inhbe* loss-of-function variants suggested a possible ligand-receptor pair [3]. In this manuscript, the ligand-receptor pairing of Activin E and ALK7 has been demonstrated genetically and biochemically. CRISPR editing of ALK7 in brown adipocytes blunted the ability of Activin E conditioned media to both increase SMAD phosphorylation and suppress NEFA release. Further, Inhbe AAV treatment failed to suppress lipolysis in ALK7 kinase deficient mice, despite reducing CL-stimulated NEFA in wildtype animals. These data are the first to directly demonstrate a functional link between the Activin E ligand and the ALK7 receptor. In addition to this direct experimental evidence, several observations from animal experiments also support a link between the ALK7 and Activin E. First, genetic inactivation of ALK7 in mice and treatment of mice with an ALK7 receptor neutralizing monoclonal antibody (mAb) increases lipolysis, similar to what is observed in INHBE KO mice [12,13,34,35]. Furthermore, genetic deletion of ALK7 increases hepatic TAG, a finding also seen with Activin E knockdown during fasting and HFD feeding [35]. A transient increase in hepatic TAG is also observed with ALK7 neutralizing mAB treatment [34]. These common effects of ALK7 and Activin E on lipolysis and hepatic TAG highlight the importance of the Activin E-ALK7 axis in liver-adipose communication. Furthermore, the phenotypic similarities observed between humans harboring loss-of-function mutations in INHBE and ALK7 strongly support the idea that the Activin E-ALK7 signaling axis is operative and biologically relevant in humans.

In adipose tissue, activation of TGF-β receptor family members influences multiple biological process capable of affecting adipose NEFA release, including adipocyte metabolism, differentiation, and adipose fibrosis [36,37]. In adipocyte precursors, activation of the TGF-β pathway inhibits adipocyte differentiation and promotes commitment of pre-adipocytes to a profibrotic, myofibrolast-like fate [38,39]. The expression of ALK7 in adipocyte precursors is low, however, and treatment of adipocyte precursors with the ALK7 ligand, Activin C, did not impact adipocyte differentiation [12,13,37,40]. Thus, if Activin E acts through ALK7 as suggested by present data, it is unlikely to influence adipocyte NEFA release by suppressing adipocyte differentiation or altering preadipocyte fate. In contrast to adipocyte precursors, the expression of ALK7 is robust in mature adipocytes where it has been shown to influence several distinct metabolic pathways capable of affecting adipocyte NEFA release [12,13,40]. First, activation of ALK7 in 3T3-L1 adipocytes by overexpression of a constitutively active receptor or treatment of primary adipocytes with ALK7 ligands, Activin B and Activin C, reduces expression of canonical lipases, including *Pnpla2* and *Hsl,* indicating that ALK7 reduces NEFA by downregulating fatty acid liberation from TAG [12,13,37]. Second, activation of ALK7 by Activin B reduces expression of the β_3 adrenergic receptor in primary adipocytes, thereby blunting adrenergic stimulation of lipolysis [13]. Finally, genetic deletion of ALK7 increases adipose mitochondrial gene expression, suggesting ALK7 also controls NEFA efflux from adipocytes through changes in fatty acid oxidation [13]. Given that ALK7 is required for suppression of adipocyte NEFA release by Activin E, it is likely that these mechanisms also mediate the actions of Activin E. In this study we observed reduced *Adbr3* expression and elevated *Ucp1* expression in mBAds treated with INHBE CM, suggesting that Activin E may reduce adipocyte NEFA efflux, in part, both by reducing sensitivity to adrenergic stimulation as well as by increasing FA oxidation secondary to uncoupled mitochondrial respiration.

Increased visceral adiposity strongly predicts risk for cardiometabolic disease [41]. This association between increased visceral adiposity and disease risk is consistent across all body mass index (BMI) categories, indicating that fat distribution rather than fat mass alone, is a primary modulator of metabolic disease [42]. Thus, strategies to reduce visceral adiposity may have therapeutic potential for the treatment of cardiometabolic disease. In human GWAS studies, *Inhbe* and ALK7 loss-of-function genetic variants associate with not only reduced visceral adiposity, but also reduced risk for metabolic disease [3,4,11,26]. These observations suggest that suppressing the Activin E-ALK7 signaling axis may be a therapeutic strategy for the treatment of metabolic disease. In support of this hypothesis, it was recently shown that targeting ALK7 with a neutralizing antibody reduces body weight gain and improves insulin sensitivity of ddY mice fed a HFD [34]. In contrast to these results, in this study genetic ablation of Activin

 © 2023 The Authors. Published by Elsevier GmbH. This is an open access article under the CC BY-NC-ND license (http://creativecommons.org/licenses/by-nc-nd/4.0/).

E in mice resulted in hepatic steatosis and insulin resistance during HFD feeding. This occurred despite significant reductions in body weight and fat mass. A similar increase in hepatic TAG and insulin resistance was also observed in ALK7 genetic knockdown mice fed HFD [35]. The reason for this discordance between mouse and human genetic phenotypes is not known. As the protection from metabolic disease observed in human INHBE and ALK7 loss-of-function variants is postulated to be secondary to reductions in visceral adiposity, differences in the distribution and function of adipose depots between species may explain these discrepant phenotypes. In line with this hypothesis, ALK7 protein abundance is markedly elevated in the epididymal fat pads of C57BL6 mice used in these studies compared to ddY mice, which show improved insulin sensitivity following ALK7 inactivation [34]. Furthermore, fasting circulating NEFA is not elevated in ddY mice lacking ALK7 while ALK7 KO mice on C57BL6 background show markedly elevated circulating NEFA relative to controls. These observations highlight how species/strain differences in the expression of ALK7 in visceral adipose may influence the magnitude of NEFA release as well as the metabolic response to inactivation of the Activin E-ALK7 axis. Additional work is required to define the adipose depot specific effects of Activin E and elucidate possible species differences in adipose depot expression of ALK7.

The reason mice lacking *Inhbe* develop insulin resistance is most likely explained by Activin E's effects on adipose tissue lipolysis. Dysregulated adipose tissue lipolysis in obesity leads to an increase in circulating NEFA [43]. This elevation in circulating NEFA is believed to contribute directly to obesity-associated insulin resistance [44]. This is supported by experimental data showing an acute infusion of exogenous NEFA into circulation causes transient insulin resistance in humans [45]. The relationship between obesity associated increases in plasma NEFA and insulin resistance is further supported by human longitudinal studies [46]. In human obesity, there is a significant correlation between increased adipocyte lipolysis and reduced insulin sensitivity. Further, in morbidly obese patients undergoing bariatric surgery the change in adipose explant lipolysis pre-vs. post-surgery directly correlated with insulin sensitivity such that patients with the greatest reduction in explant lipolysis showed the strongest improvements in insulin sensitivity [46]. These data support the hypothesis that disruption of Activin E signaling by genetic ablation of *Inhbe* increases adipose lipolysis, leading to an increase in circulating NEFA, which contributes directly to insulin resistance in these mice. More broadly, these observations suggest that the Activin E liver-adipose axis is critical to maintain normal adipose lipolysis and overall metabolic homeostasis.

While this manuscript was in preparation, Adam et al. reported that adenovirus mediated Activin E overexpression in mice reduced fasting NEFA in an ALK7 dependent manner [47]. In addition, the authors demonstrated that genetic loss of Activin E in mice increased lipolysis and reduced fat mass during HFD feeding, but resulted in elevated hepatic TAG and insulin resistance. These results are consistent with our studies and support the hypothesis that the Activin E-ALK7, liver-adipose signaling axis regulates adipose lipolysis and metabolic health.

3.1. Conclusions

In summary, our studies highlight an inter-organ communication loop between liver and adipose requiring the TGF-β ligand, Activin E. Our data support a model in which hepatic Activin E is increased in response to elevated NEFA, TAG or both, and acts as an hepatokine to suppress adipose lipolysis in an ALK7 dependent manner. Using a mouse model of *Inhbe* knockout, we demonstrate that the Activin E-ALK7 signaling axis is critical for maintaining metabolic homeostasis.

3.2. Limitations

Investigation of Activin E's influence on cell function is presently limited by a lack of readily available purified protein. We have attempted to overcome this obstacle by generating media enriched with Activin E – specifically by over-expressing INHBE, a non-signaling peptide monomer which dimerizes to form the signaling competent Activin E [7]. While we found INHBE to be enriched in our conditioned media, other activin monomers were also detected at low concentrations (data not shown). The presence of additional activin monomers in conditioned media has important implications for interpretation of CM experiments as activin heterodimers composed of INHBE and other activin isoforms have been identified using in-vitro overexpression experiments [10]. However, the signaling capacity and function of INHBE heterodimers is poorly understood. Thus, while our CM depletion experiments strongly suggest the actions of INHBE CM are due to Activin E, we cannot fully rule out a contribution from other INHBE containing Activin heterodimers.

While these data support the necessity of ALK7 for Activin E mediated SMAD phosphorylation and lipolytic suppression *in vitro*, as well as suppression of fasting and CL stimulated free fatty acid release *in vivo*, we have not demonstrated a direct ligand-receptor binding relationship. It is possible that Activin E's actions are mediated indirectly by the ALK7 receptor.

Although *Inhbe* expression is highly enriched in the liver of both mice and humans, *Inhbe* transcript is detectable in adipose tissue (Supplemental Fig. S10A). Thus, we cannot rule out the possibility that loss of *Inhbe* in the adipose tissue, or other extrahepatic tissues, may contribute to the metabolic phenotype of the *Inhbe* global knockout mice.

4. MATERIALS & METHODS

4.1. Resource availability

4.1.1. Lead contact

Further information and requests for resources and reagents should be directed to and will be fulfilled by the lead contact, John D. Griffin (John.Griffin@pfizer.com).

4.1.2. Materials availability

The availability of animal lines and plasmids generated in these studies is restricted. Distribution will require a materials transfer agreement prior to distribution.

4.1.3. Data and code availability

All data reported in this paper will be shared by the lead contact upon request. This paper does not report original code. Any additional information required to reanalyze the data reported in this paper is available from the lead contact upon request.

4.2. Experimental model & subject details

4.2.1. Animal welfare

All procedures performed in animals were in accordance with regulations and established guidelines and were reviewed and approved by an Institutional Animal Care and Use Committee.

4.2.2. Generation of INHBE KO mice

Mice deficient for the *Inhbe* gene were generated utilizing CRISPR/Cas9 technology and maintained on a C57BL/6J background [48]. Knockout of the gene was achieved by deleting ~1.4 kb genomic

 © 2023 The Authors. Published by Elsevier GmbH. This is an open access article under the CC BY-NC-ND license (http://creativecommons.org/licenses/by-nc-nd/4.0/).

region that contains the entire coding sequence and intervening intron (ENSMUST00000059718.6). Two Cas9 guides targeting exon 1 (5′-CTGCTTTGAGAACCTCGAAT) and exon 2 (5′-ACTCGAGCTTCCAGACACGT), respectively, were designed for efficient editing while minimizing potential risk of off-target editing. To generate F0 mice, 1-cell embryos were harvested from superovulated females, electroporated with the two sgRNAs complexed with Cas9 protein and implanted into pseudo-pregnant recipients. Live pups born from implanted embryos were genotyped by PCR amplification with primers, 5′-CCCTGCCAGTAGTTAGTCATG and 5′- ACTTCTTTCTCGGGAGAGAC, followed by Sanger sequencing. Selected founders were bred with wild-type C57BL/6J mice for germline transmission of knockout alleles. Subsequently, confirmed heterozygous mice were further bred to establish a colony.

4.2.3. Generation of ALK7 kinase inactive (K222R) mice

The K222R mutation was introduced into the exon 4 of the mouse *ALK7* (*Acvr1c*) gene in the in-house transgenic facility utilizing the CRISPR/Cas9 technology 2013 [48]. A sgRNA (protospacer: 5′-CTGTGAAAATATTCTCCTCC) that targets the K222 position in the genome was complexed with Cas9 protein and electroporated into C57BL/6J 1-cell embryos together with an oligo donor containing the missense mutation (A > G, underlined), 5′-GGAAAAGGTCGGTTTGGGGAAGTGTGGCACGGAAGATGGTGTGGAGAAGATGTGGCTGTGAGAATATTCTCCTCCAGGGATGAGAGATCTTGGTTCCGTGAGGCGGAAATTTATCAGACGGTG. Embryos were then transferred to pseudo-pregnant females to generate live pups. Potential founders were genotyped by genomic PCR (primers: 5′-TACAGTTGGTTGTAATGATGC and 5′-TACGTCATCATGACTCTACACC) followed by Sanger sequencing. Selected founders carrying the K222R mutation were bred with wildtype C57BL/6J mice for germline transmission.

4.2.4. Generation of ALK7 constitutively active (ALK7 CA) mice

The ALK7 constitutively active T194D mutation (ACA > GAC) was introduced into the exon 4 of the mouse *ALK7* (*Acvr1c*) gene in the in-house transgenic facility utilizing the CRISPR/Cas technology [12,48]. For genome editing, a Cpf1 crRNA with a protospacer (5′-TTGAAGTACAATTGTCCTTGC), A.s. Cas12a (Cpf1) Ultra (IDT) and an oligo DNA donor (CCATCTTCCGTGCCACACTTCCCCAAACCGACCTTTTCCTACGATTTCTTGAAGTACAATGTCCCTTGCGATTGTTCTTTGAACCAAGAGAGGCAGACCTAGTCAAAGAAAGGGCAGCCTGAT) were delivered to C57BL/6J 1-cell embryos via pronuclear injection. Embryos were then transferred to pseudo-pregnant females to generate live pups. Potential founders were genotyped by genomic PCR (primers: 5′-TACAGTTGGTTGTAATGATGC and 5′-TACGTCATCATGACTCTACACC) followed by Sanger sequencing. Selected founders carrying the T194D allele were bred with wildtype C57BL/6J mice for germline transmission.

4.2.5. AAV8 mediated INHBE over-expression

The coding sequence for mouse (NM_008382.3) Inhbe prepropeptide was inserted into an AAV8 adenoviral backbone under the control of the hepatocyte restricted thyroxine binding globulin (TBG) promoter (AAV8-TBG). 8 week old wildtype, male mice were injected retro-orbitally with 3×10^{11} genome copies of AAV8-TBG coding Inhbe (Inhbe AAV) or, as a control, 3×10^{11} genome copies of AAV8-TBG coding empty vector (EV AAV). In some experiments an additional control arm was employed by treating mice with 100ul of saline only.

4.2.6. Immortalized mouse Brown adipocyte culture

Immortalized mouse primary brown adipocytes (mBAd) were a gift from Dr. Patrick Seale (Perelman School of Medicine, University of Pennsylvania) [49]. Cells were maintained at 37 °C, 5 % relative humidity in growth medium consisting of DMEM high glucose, 10 % fetal bovine serum, and 1 % penicillin-streptomycin. Cultures were passaged prior to reaching 80 % confluence. For differentiation, cells were seeded at 18,000 cells/cm^2 in growth medium and allowed to reach confluence for 4 days. At confluence, cells were induced to differentiate for two days in induction media (growth media supplemented with 1 nM 3,3′,5-Triiodo-L-thyronine (T_3), 20 nM insulin, 500 μM IBMX, 1 μM dexamethasone, and 125 μM indomethacin). Following induction, media was changed to differentiation media (growth media supplemented with 20 nM insulin and 1 nM T_3). Fully differentiated adipocytes were obtained 7—8 days after starting differentiation.

4.2.7. Isolation, culture, and differentiation of mouse primary adipocytes

Adipocyte precursors were isolated from the subcutaneous depots of 12 week old male ALK7 K222R mice as previously described [50]. In brief, adipose depots were excised under sterile conditions, rinsed in sterile 37 °C PBS, and then added to 5 mL of 37 °C adipocyte isolation buffer consisting of Krebs Ringer HEPES buffer (117 mM NaCl, 4.7 mM KCl, 2.5 mM CaCl2, 1.2 mM MgSO4, 24.6 mM NaHCO3, 5 mM HEPES, pH 7.3) containing 4 % BSA and 5 mM glucose. Tissue was minced, added to 5 mL of isolation buffer containing 5 mg collagenase and digested in a 37 °C shaking water bath for 45—60min. Digested solution was then filtered through a 100uM nylon filter into a 15 mL conical tube and centrifuged for 5min at 50g. The floating adipocyte fraction was removed and discarded. The stromal vascular fraction (SVF) containing preadipocytes was then pelleted by 450g × 5min centrifugation at 4C. Red blood cells (RBC) were lysed as described using lysis media (155 mM NH4Cl, 10 mM KHCO3, 0.1 mM EDTA). Following RBC lysis, media was passed through a 40uM filter and SVF was pelleted as above at 4C. Media was discarded and isolated adipocyte precursors were resuspended in plating media. Adipocyte precursors from SVF isolation were plated at 25,000cells/cm^2 and maintained at 37 °C and 5 % CO2. Media was changed the day following isolation and every other day thereafter until cells reached confluence. At confluence, differentiation media (DMEM/F12 supplemented with 5 % FBS, 17 nM insulin, 0.1 μM dexamethasone, 250 μM IBMX, and 60 μM indomethacin) was added. After 2 days, media was changed to maintenance media (DMEM/F12, 5 % FBS and 17 nM insulin). Partial, 50 % media changes were performed every two days thereafter. Fully differentiated adipocytes were observed 6—8 days following addition of differentiation media.

4.2.8. Huh7 culture

Huh7 hepatocellular carcinoma cells were cultured in growth media containing DMEM high glucose supplemented with 10 % FBS, 1 % Glutamax, 1 % Na Pyruvate, 1 % 1 % Penicillin/Streptomycin at 37 °C and 5 % CO_2. Cells were routinely passaged at 80 % confluence and seeded at 10,000 cells/cm^2 for expansion. Cells between passage 15 and 20 were used for experiments.

4.2.9. HEK293T culture

HEK293T were cultured in growth media containing DMEM high glucose supplemented with 10 % FBS, 1 % NEAA, 1 % Glutamax, 1 % Na Pyruvate, 1 % 1 % Penicillin/Streptomycin at 37 °C and 5 % CO_2. Cells were routinely passaged at 80 % confluence and seeded at 20,000 cells/cm^2 for expansion. Cells between passage 10 and 20 were used for experiments.

 © 2023 The Authors. Published by Elsevier GmbH. This is an open access article under the CC BY-NC-ND license (http://creativecommons.org/licenses/by-nc-nd/4.0/).

4.2.10. HEK293SBE reporter culture

HEK293 cells stably expressing a luciferase reporter gene linked to a SMAD binding element (SBE) promotor were cultured according to manufacturer's instructions. Cells were grown in growth media consisting of MEM supplemented with 10 % FBS, 1 % non-essential amino acids, 1 mM Na pyruvate, 1 % Penicillin/Streptomycin and 400 μg/mL of Geneticin at 37 °C and 5 % CO_2. Cells were routinely passaged at 80 % confluence and seeded at 20,000cells/cm^2 for expansion. Cells between passage 5 and 10 were used for experiments.

4.3. Method details

4.3.1. Plasma metabolites

Glucose was routinely measured from blood collected by tail vein nick using glucometer. Plasma insulin was determined by immunoassay from blood drawn from tail or submandibular vein. For plasma free fatty acids blood was collected from either tail vein or submandibular vein, as indicated in figure legends, and free fatty acids were determined enzymatically.

4.3.2. Hepatic TAG

Frozen livers were pulverized under liquid nitrogen. 30–50 mg liver was homogenized in a 15× volume/weight ratio of ice cold triglyceride extraction buffer (10 mmol/L TRIS, pH 7.4, 0.9 % NaCl, and 0.2 % Triton X-100) using a Qiagen Tissue Lyser 2 at 4 °C using 2 cycles of 30hz × 2min. Triglycerides were analyzed immediately following homogenization using a Siemens Chemistry XPT clinical analyzer.

4.3.3. In vivo lipolysis

Lipolysis was assessed by determining free fatty acid concentrations in plasma isolated from mouse tail vein blood. For fasting-refeeding lipolysis studies, mice were housed in reverse light–dark cycle rooms at 28 °C and blood was collected 4hrs following the start of the dark cycle, representing the ad-libitum fed state. Mice were then moved to fresh cages without food and blood was collected again after 6hr and 18hr of fasting. Where indicated, following an overnight fast chow diet was reintroduced for 4hrs and an additional blood sample was collected. For stimulated lipolysis experiments, a baseline bleed was collected in the ad-libitum fed state, as above. Food was then removed and mice were injected intraperitoneally with 100 μg/kg of 20 ng/μL CL316,243 dissolved in sterile saline and tail vein blood was collected at indicated timepoints. Where indicated, following collection of tail vein blood, animals were euthanized via CO2 asphyxiation, liver was collected and flash frozen in nitrogen for determining hepatic triglyceride and measuring gene expression. Prior to all experiments, mice were randomized into individual cages and researchers were blinded by removing group identifiers from cages.

4.3.4. Incubation of Huh7 cells with fatty acids

Ethanol solubilized fatty acids (FA) from the manufacturer were dried under nitrogen gas and FA sodium salts were generated by solubilizing dried FA in PBS containing 1/100th volume of 1N sodium hydroxide to a final concentration of 20 mM. On the day of the experiment, FA were complexed to BSA by mixing a solution containing FA sodium salt at 10× final concentration with serum free culture media containing fatty acid free BSA at a concentration of 1.6 mM (11 % BSA solution). Thus, the FA:BSA complexing ratios for oleate concentrations used in experiments were 2:1 (334 μM), 3:1 (500 μM), 4:1 (668 μM), and 5:1 (835 μM). For palmitate the FA:BSA complexing ratios were 0.25:1 (42 μM), 0.5:1 (84 μM), 1:1 (167 μM), and 2:1 (334 μM). After mixing at 37 °C for 30min, FA:BSA complexed solutions were diluted with cell culture media containing 1 % FBS (1.1 % BSA final concentration).
One day prior to experiment, Huh7 cells at 80 % confluence were rinsed once in PBS and starved overnight in starvation media (DMEM high glucose, 1 % FBS, 1.1 % BSA, 1 % Glutamax, 1 % Na Pyruvate, and 1 % Penicillin/Streptomycin). On the day of the experiment, starvation media was replaced with FA containing media. Cells were incubated with FA containing media for 24hrs. At the end of the experiment media was removed and cells were flash frozen on liquid nitrogen.

4.3.5. Generation and use of INHBE conditioned media

To generate media enriched for INHBE, 3 × 10^6 Expi293F cells were seeded into 1L Expi293 media and grown in a suspension culture system maintained at 36 °C and 8 % CO2. One day after seeding, a transfection solution was prepared by combining 1.3 mg of pcDNA3.1 plasmid containing the mouse (NM_008382.3) or human (NM_031479.5) Inhbe prepropeptide coding sequence with 2.6 mg polyethyleneimine in 100 μl Opti-Mem and added directly to culture media. 3hrs following transfection, culture media was supplemented with valporic acid and heparin to final concentrations of 3 mM and 2 μg/mL, respectively. 96hr after transfection, the suspension culture was harvested and clarified by centrifugation at 3,000g × 10min. Clarified media was passed through a 0.2 μM filter and this conditioned media (CM) stored at −80C prior to use.
For CM experiments, treatment media containing conditioned media was prepared for each step of the assay by combining (1 volume * x/100) conditioned media with (0.5 volumes) experimental media containing 2× concentration of supplements and (1 volume * (100-x)/100) of experimental media without supplements. Thus, concentrations of media supplements (i.e.: fetal bovine serum, antibiotics) were kept consistent between control experimental media and treatment media spiked with CM.

4.3.6. Depletion of INHBE in conditioned media

50ul of 30 mg/mL Protein G Dynabeads were washed and resuspended in pulldown media (KRBH media supplemented with 1 % BSA) and either 20 ng of anti-human Activin E antibody or 20 ng of Rabbit IgG. A solution of 0.05 % proclin and 50 % glycerol was added to Rabbit IgG groups at the necessary volume to control for the anti-human Activin E antibody vehicle. Solutions were mixed with beads for 10min at 4C on a rotating rocker. Antibody media was discarded and beads were washed 3× with ice cold pulldown media by gentle pipetting. 700 μl of cold pulldown media containing 33 % conditioned media was then added to beads and mixed for 30min at 4C on a rotating rocker. Where indicated, 75 ng/mL Activin B was spiked into EVCM pulldown groups. After 30min, media was removed and placed on ice. Beads were washed twice in cold PBS and flash frozen on nitrogen.
Depleted media was diluted to a 10 % final concentration for adipocyte lipolysis experiments and 5 % final concentration for HEK293SBE signaling experiments (described below).

4.3.7. LC/MS–MS quantification of INHBE in conditioned media

4.3.7.1. Protein precipitation and digestion. Following immunoprecipitation, an aliquot of conditioned media was treated with ice-cold acetone, followed by overnight incubation at −20 °C to precipitate the protein fraction. Protein was pelleted by centrifugation at 14,000 rcf for 5 min at 10 °C, followed by reconstitution with 50 μL of 8M urea/0.1M Tris, pH 8.5. Sonication was employed to fully resuspend

 © 2023 The Authors. Published by Elsevier GmbH. This is an open access article under the CC BY-NC-ND license (http://creativecommons.org/licenses/by-nc-nd/4.0/).

the protein. Samples were then reduced with DL-Dithiothreitol to a final concentration of 10 mM and allowed to incubate for 30 min at room temperature. Cysteine residues were then alkylated by addition of 2-iodoacetamide, which was added to a final concentration of 55 mM, followed by incubation for 30min at room temperature while protected from light. LysC (1 μg) was then introduced, and digestion was allowed to occur for 2 h at room temperature. Finally, urea was diluted to 1.5M with ammonium bicarbonate, followed by addition of trypsin (2.5ug). Digestion was allowed to proceed for 16 h at 37 °C.

4.3.7.2. Peptide cleanup. The following morning, the digest was desalted on a Strata-X Polymeric Reversed-Phase cartridge, using a Tecan Resolvex A200 for liquid handling. Briefly, cartridges were conditioned in the following sequence: i) Methanol, ii) 70 % Acetonitrile/0.1 % Formic Acid, iii) 0.1 % Trifluoroacetic Acid, iv) 0.1 % Trifluoroacetic Acid. Peptide digest was then added to the cartridge, followed by 0.1 % Trifluoroacetic Acid. Desalted peptides were then eluted by 70 % Acetonitrile/0.1 % Formic Acid and subsequently dried under vacuum.

4.3.7.3. Peptide quant, final cleanup, and queuing. Peptides were reconstituted in water prior to quantification by colorimetric assay. Samples were then diluted to a concentration of 1 μg/μL in water. A 20 μg aliquot was then subjected to chemical labeling with TMT-Pro reagent according to manufacturer's instructions. After the labeling reaction, samples were pooled according to manufacturer's instructions. A 20 μg aliquot of pooled, labeled peptides was dried under vacuum, followed by reconstitution in 0.1 % Trifluoroacetic acid. Peptides were fractionated by reversed-phase high-pH fractionation according to manufacturer's instructions. The resulting eight fractions were then dried under vacuum prior to reconstitution in 20 μL of 5 % Acetonitrile/0.1 % Formic Acid. Samples were briefly sonicated and then transferred to autosampler vials.

4.3.7.4. LC-MS/MS. Samples were held at 4 °C in the autosampler of an EASY-nLC 1200 liquid chromatography system. Upon injection, a 10 μL volume was transferred to an EASY-Spray column composed of C18 stationary phase. Peptides were eluted over the course of 110 min using a binary solvent system composed of 0.1 % Formic Acid (Solvent A) and 80 % Acetonitrile/0.1 % Formic Acid (Solvent B). Briefly, the proportion of Solvent B was increased linearly from 3 % to 30 % over 100min, followed by a linear increase from 30 % to 60 % over the subsequent 10min. The column was then subjected to 100 % Solvent B before restoration of starting conditions ahead of the next injection, for a total analysis time of 125min.

The EASY-nLC system was coupled to a Thermo Q Exactive HF mass spectrometer. A 'Top 10' data-dependent acquisition method was employed with the instrument set in positive detection mode. For MS1, resolution was set to 60,000, the scan range was set to 350−1800 *m/z*, and the AGC target was set to 5e5, with a maximum IT of 50 ms. For MS2, resolution was set to 60,000, the normalized CE was set to 38, the isolation window was set to 0.7 *m/z*, the AGC target was set to 1e5, and the maximum IT was set to 105 ms.

Raw files were analyzed using the Sequest algorithm (SEQUEST HT, Thermo Scientific) within Proteome Discoverer 2.4 against the UniProt human database. A 10ppm MS1 error tolerance was used. Trypsin was set as the enzyme, allowing for 2 missed cleavages. TMT tags on lysine residues and peptide N-termini (229.162932 Da) and carbamidomethylation of cysteine residues (57.02146 Da) were set as static modifications, while oxidation of methionine residues (+15.99492 Da) and acetylation of peptide N-termini (42.011 Da) were set as variable modifications. Percolator was used as the false discovery rate calculator, and all peptides were filtered at the "Strict" Target FDR level of 0.01. Mouse INHBE was quantified by the reporter ion intensities for the peptide 'ANNPWPAGSSCCVPTAR', which was detected at 2149.0238 *m/z*. Human INHBE was quantified by the reporter ion intensities for the peptide 'RTPTCEPATPLCCR', which was detected at 2022.9842 *m/z*.

4.3.8. Adipocyte lipolysis

Lipolysis experiments were performed on adipocytes 7−9 days following start of differentiation. For all lipolysis experiments adipocytes were pretreated with differentiation media spiked with conditioned media for 24hrs prior to assay. Following 24hr pre-treatment, cells were starved for 3hrs in DMEM high glucose containing 1 % bovine serum albumin (BSA) final concentration with or without CM. Cells were then rinsed once in neat KRBH buffer prior to addition of 0.9 volumes of lipolysis assay buffer (KRBH supplemented with 3 % fatty acid free BSA, 10 mM glucose) with or without CM. 0.1 volumes of KRBH containing 10× final concentration of lipolysis reagents was then added to wells, plates were rocked gently, and cells were incubated at 37C for 2hrs. Media was then collected, centrifuged 1,500g × 5min at 4C to pellet residual cell debris, and fatty acid concentration of the supernatant were determined enzymatically.

Cellular cAMP concentrations following ligand stimulation were determined by competitive immunoassay following manufacturer's instructions (Cisbio, Cat# 62AM4PEB). Briefly, mBAD were pre-treated and starved in 3 % CM solutions as performed for lipoysis experiments. Following starvation cells were incubated at 37 °C in assay media (Hanks Buffered Salt Solution, 5 mM HEPES, 1 % fatty acid free BSA, and 500 μM IBMX) containing 3 % final concentrations of conditioned media. After 45min, isoproterenol, CL 316,243, or forskolin were added at the indicated concentrations and cells were incubated for an additional 30min. Media was then supplemented with cAMP-d2 and cAMP-cryptate solutions, incubated at 37 °C for 1hr, and fluorescence was analyzed using a Perkin Elmer EnVision multimode plate reader.

4.3.9. HEK293T SMAD signaling

Experiments to measure the SMAD signaling response of HEK293T to CM treatment were repeated as previously described [26]. In brief, 200,000 HEK293T cells in DMEM High Glucose supplemented with 10 % FBS, 1 % NEAA, 1 % Glutamax, 1 % Na Pyruvate, and 1 % antibiotics were seeded onto to polyethylenimine coated 12 well plates 24hrs prior to transfection. Cells were transfected overnight with 1 μg pcDNA3.1 plasmid DNA containing either empty vector, wildtype human ALK7, or 0.5 μg of the Activin co-receptor, Cripto, using Lipofectamine 2000 following kit instructions.

Following transfection cells were rinsed once and then incubated in pre-treatment media (DMEM High Glucose, 0.5 % FBS, 1 % NEAA, 1 % Glutamax, 1 % Na Pyruvate, 1 % antibiotics) for 24hrs. Following pre-treatment incubation, cells were rinsed in assay media (DMEM High Glucose, 0.5 % FAF-BSA, 1 % NEAA, 1 % Glutamax, 1 % Na Pyruvate, 1 % antibiotics, final concentrations) then treated with or without 10 μM of the ALK4/5/7 kinase inhibitor SB431542 for 3hr. DMSO was used as a vehicle control in untreated cells. At the end of the 3hr incubation, media was removed and fresh assay media was added containing a final concentration of 30 % conditioned media. Where indicated, 25 ng/mL Activin B was added to EVCM. In addition, 10 μM SB431542 or DMSO vehicle was co-incubated with ligands where indicated. After 30min of incubation cells were rinsed briefly in ice cold PBS and plates were flash frozen by floating on liquid nitrogen. Frozen plates were stored at −80C until processing for western blotting.

 © 2023 The Authors. Published by Elsevier GmbH. This is an open access article under the CC BY-NC-ND license (http://creativecommons.org/licenses/by-nc-nd/4.0/).

SMAD2/3 activation was assessed by the ratio of phosphorylated SMAD protein abundance to total SMAD protein abundance. For each experimental replicate, abundance ratios were normalized to EV transfected cells treated with EVCM group.

4.3.10. HEK293SBE SMAD signaling

HEK293 cells stably expressing a luciferase reporter gene linked to a SMAD binding element (SBE) promoter were cultured according to manufacturer's instructions. For transfection, 35,000 cells were seeded onto polyethylenimine coated 96 well, white, clear bottom plates in growth media. 24hrs following plating, cells were transfected with plasmids coding containing EV or human ALK7 as described above. After overnight transfection, cells were rinsed once in growth media, and then incubated for 24hr in growth media supplemented with CM. Where indicated, 25 ng/mL Activin B was added to EVCM. Following 24hr of CM incubation, 1 volume of One-Glo luciferase detection reagent was added to cells, a white adhesive plate cover was added to the bottom of the plate to allow detection of luminescence, and plates were shaken for 5min at RT to facilitate lysis. After 5min, luminescence was read on a Spectramax M5.

4.3.11. Transfection of mBAd with RNP for CRISPR mediated gene editing

Transfection of mBAd fibroblasts with ribonucleoprotein (RNP) complexes was performed using the 100 μl Neon Transfection System as previously described with minor modifications [51]. In brief, cultures of sub-confluent primary mouse brown adipocyte precursors were trypinsized, washed in PBS, and resuspended in Neon Transfection Buffer R at 10-20 $\times$ 10^6 cells/mL. Concentrated RNP complex solution was prepared by combining 6 μM sgRNA and 8uM S.p. Cas9 Nuclease in Buffer R. The cell suspension was then mixed with an equal volume of concentrated RNP complex by gentle pipetting. 100 μl of RNP-cell mixture was loaded into the Neon Transfection tip and cells were electroporated using a single 30 ms pulse of 1350 mV. Immediately following electroporation, cell suspension was diluted in warm growth media and plated. Cells were grown to confluence and differentiated using standard conditions.

4.3.12. mBAd & mouse primary adipocyte SMAD signaling

Fully differentiated mouse brown adipocytes and primary adipocytes were starved for 3hrs in DMEM High Glucose containing 1 % BSA final concentration. Following starvation, cells were treated with starvation media containing a 30 % final concentration of CM. Where indicated, 25 ng/mL Activin B was spiked into EVCM treatment groups. 30min after addition of CM, media was removed, cells were rinsed twice in ice cold PBS, and plates were flash frozen on liquid nitrogen. Frozen plates were stored at −80C for western blotting.

4.3.13. Western blotting

Cells were lysed in ice cold TNET-C Buffer containing phosphatase and protease inhibitors. Lysate was homogenized using sonication and clarified by centrifugation at 12000*g* for 15min at 4C. Protein concentrations were determined by BCA Assay. Cell homogenate was denatured using NuPage sample buffer and reducing reagents and heating at 70 °C for 10min. 10 μg of sample was loaded on 4−12 % Bis-Tris Gels and separated at 130V for 100min using Invitrogen NuPage Running Buffer and the Biorad Criterion electrophoresis system. After electrophoresis gels were incubated in ice cold NuPage transfer buffer containing 10 % methanol for 15min. Proteins were transferred onto nitrocellulose membranes on ice at 100V for 60min using the Biorad Criterion transfer system with plate electrodes. Following transfer membranes were blocked for 1hr in 5 % milk, used with pSMAD3 blots, or LICOR blocking reagent, for pSMAD2, ALK7 and Cripto blots, and incubated with indicated antibodies overnight at 4C. Densities were quantified using Biorad ImageLab software or ImageJ.

4.3.14. RNA isolation and real-time qPCR

RNA extraction was performed following previously described methods [52]. In brief, 700 μl of ice cold Triazol reagent was added to wells of frozen adipocytes. Tissue was homogenized in Triazol using the Qiagen Tissue Lyser 2 with two 1' x 30hz runs. Following homogenization 140 μl of chloroform was added to homogenate and mixed by inversion. Samples were centrifuged at 12,000g $\times$ 15min to separate phases. The aqueous phase was collected, combined with another 140 μl of chloroform, mixed, and centrifuged as above. Aqueous phase was again collected and combined with 250 μl cold isopropanol. Sample was mixed by inversion and 1 μl of RNA-grade glycogen was added as a carrier. RNA was precipitated overnight at −20 °C. Precipitated RNA was collected by centrifuging at 12,000g for 10min at 4C. Isopropanol was removed and pellets were washed three times in cold, 75 % ethanol. Following washing pellets were air dried for 10min at RT, and then again for 2min at 60 °C on a heating block. Dried pellets were solubilized by adding 20 μl of ddH20 and incubating at 60 °C for 2min. Samples were then placed on ice and RNA concentration was determined using a Nanodrop spectrophotometer.

cDNA was generated from extracted RNA using High-Capacity cDNA Reverse Transcription kit per kit instructions. Following reverse transcription cDNA was diluted to a final concentration of 10 μg/μl qPCR was performed using Applied Biosystems SYBR or Taqman reagents per kit instructions with primers listed in Table S1 and Table S2. Relative expression was quantified by the Pfaffl Method [53].

4.3.15. Metabolic phenotyping

For INHBE KO metabolic phenotyping studies, 8 week old mice were individually housed at thermoneutrality and randomly assigned to chow or 60 % high fat diet (HFD). Wildtype littermates were used as controls. Body weights were measured weekly. Body composition was determined by Echo MRI imaging following 11 weeks of diet feeding. Blood was drawn from submandibular vein using a lancet after a 6hr fast at 3 and 6 weeks of diet feeding and plasma was used for measuring insulin and NEFA. Blood glucose was sampled from tail vein at this time. HOMA-IR was calculated using glucose and insulin values from 6hr fasting mice. An insulin tolerance test (ITT) was performed after 4 weeks on diet by intraperitoneal injection of insulin solution in saline. Chow mice received 0.5UI/kg and HFD fed mice received 0.75UI/kg. Glucose was measured from the tail vein at baseline and indicated timepoints following insulin injection. ITT data are expressed as mean blood glucose over time. When significant differences in baseline glucose were observed, change in glucose from baseline was calculated for each time point and group mean change in glucose was presented. AUC was calculated using the trapezoidal rule. Mice were euthanized following a 6hr fast and tissues were flash frozen in nitrogen prior to processing.

4.4. Quantification and statistical analysis

Results are expressed as means ± S.E.M. Student's t tests were performed to compare differences between two groups. For experiments in which multiple comparisons were made to a within factor control (i.e.: HEK293T SMAD signaling experiments: experimental transfection group vs. EV transfection control within CM treatment group) a one-way ANOVA with Dunnett's post-hoc testing was

 © 2023 The Authors. Published by Elsevier GmbH. This is an open access article under the CC BY-NC-ND license (http://creativecommons.org/licenses/by-nc-nd/4.0/).

performed. For two factor studies, data were analyzed using a two-way ANOVA followed by Tukey's HSD post-hoc testing. For time series data, such as body weight and insulin tolerance testing, group comparisons were performed within each time point. Statistical analyses were conducted using Prism 9 software. A value of $p < 0.05$ was considered statistically significant.

AUTHOR CONTRIBUTIONS

J.D.G.: Conceptualization, Methodology, Validation, Formal Analysis, Investigation, Resourcing, Writing — Original Draft, Writing — Review & Editing, Visualization. **J.B:** Conceptualization, Methodology, Validation, Formal Analysis, Investigation, Resourcing, Writing — Review & Editing. **J.C.:** Methodology, Validation, Formal Analysis, Investigation, Resourcing, Writing — Original Draft, Writing — Review & Editing. **R.B.:** Investigation. **E.A.J**.: Investigation. **A.R.W.:** Investigation. **S.E.F:** Investigation. **B.B.:** Conceptualization, Methodology, Validation, Formal Analysis, Investigation, Resourcing, Writing — Review & Editing, Supervision, Project Administration. **T.R.:** Conceptualization, Methodology, Validation, Formal Analysis, Investigation, Resourcing, Writing — Review & Editing, Supervision, Project Administration. **K.K.B.:** Conceptualization, Methodology, Validation, Resourcing, Writing — Review & Editing, Supervision, Project Administration. **M.J.B.:** Conceptualization, Methodology, Validation, Resourcing, Writing — Original Draft, Writing — Review & Editing, Supervision, Project Administration.

DATA AVAILABILITY

Data will be made available on request.

ACKNOWLEDGEMENTS

We thank D. Archambault, M. Granade, R. Poskanzer, A. Lau and G. El Sebae for assistance with animal tissue collection. We thank Y. Ahn for assistance developing the animal models. We thank the Biomedicine Design Team including L. Mosyak, E. LaVallie, W. Stochaj, L. Racie, C. Connors, E. Longo, L. DiBlasio-Smith, C. Corcoran, J. Min-DeBartolo, and L. Lin for generation of the INHBE conditioned media.
This work was funded by Pfizer. J.D.G. was funded by the Pfizer Worldwide Research, Development and Medical Postdoctoral Program.

DECLARATION OF COMPETING INTEREST

The authors declare the following financial interests/personal relationships which may be considered as potential competing interests: All authors were employees of Pfizer when they contributed to the work reported in this manuscript.

APPENDIX A. SUPPLEMENTARY DATA

Supplementary data to this article can be found online at https://doi.org/10.1016/j.molmet.2023.101830.

REFERENCES

[1] Priest C, Tontonoz P. Inter-organ cross-talk in metabolic syndrome. Nat Metab 2019;1(12):1177—88. https://doi.org/10.1038/s42255-019-0145-5.

[2] Jensen-Cody SO, Potthoff MJ. Hepatokines and metabolism: deciphering communication from the liver. Mol Metabol 2020;44:101138. https://doi.org/10.1016/j.molmet.2020.101138.

[3] Deaton AM, Dubey A, Ward LD, Dornbos P, Flannick J, Yee E, et al. Rare loss of function variants in the hepatokine gene INHBE protect from abdominal obesity. Nat Commun 2022;13(1):4319. https://doi.org/10.1038/s41467-022-31757-8.

[4] Akbari P, Sosina OA, Bovijn J, Landheer K, Nielsen JB, Kim M, et al. Multiancestry exome sequencing reveals INHBE mutations associated with favorable fat distribution and protection from diabetes. Nat Commun 2022;13(1):4844. https://doi.org/10.1038/s41467-022-32398-7.

[5] Sugiyama M, Kikuchi A, Misu H, Igawa H, Ashihara M, Kushima Y, et al. Inhibin βE (INHBE) is a possible insulin resistance-associated hepatokine identified by comprehensive gene expression analysis in human liver biopsy samples. PLoS One 2018;13(3):e0194798. https://doi.org/10.1371/journal.pone.0194798.

[6] Hashimoto O, Funaba M, Sekiyama K, Doi S, Shindo D, Satoh R, et al. Activin E controls energy homeostasis in both Brown and white adipose tissues as a hepatokine. Cell Rep 2018;25(5):1193—203. https://doi.org/10.1016/j.celrep.2018.10.008.

[7] Hashimoto O, Tsuchida K, Ushiro Y, Hosoi Y, Hoshi N, Sugino H, et al. cDNA cloning and expression of human activin βE subunit. Mol Cell Endocrinol 2002;194(1):117—22. https://doi.org/10.1016/S0303-7207(02)00157-0.

[8] Fang J, Wang SQ, Smiley E, Bonadio J. Genes coding for mouse activin beta C and beta E are closely linked and exhibit a liver-specific expression pattern in adult tissues. Biochem Biophys Res Commun 1997;231(3):655—61. https://doi.org/10.1006/bbrc.1997.6162.

[9] Chabicovsky M, Herkner K, Rossmanith W. Overexpression of activin βC or activin βE in the mouse liver inhibits regenerative deoxyribonucleic acid synthesis of hepatic cells. Endocrinology 2003;144(8):3497—504. https://doi.org/10.1210/en.2003-0388.

[10] Wada W, Medina JJ, Kuwano H, Kojima I. Comparison of the function of the β_C and β_E subunits of activin in AML12 hepatocytes. Endocr J 2005;52(2):169—75. https://doi.org/10.1507/endocrj.52.169.

[11] Emdin CA, Khera AV, Aragam K, Haas M, Chaffin M, Klarin D, et al. DNA sequence variation in ACVR1C encoding the activin receptor-like kinase 7 influences body fat distribution and Protects against type 2 diabetes. Diabetes 2019;68(1):226—34. https://doi.org/10.2337/db18-0857.

[12] Yogosawa S, Mizutani S, Ogawa Y, Izumi T. Activin receptor-like kinase 7 suppresses lipolysis to accumulate fat in obesity through downregulation of peroxisome proliferator—activated receptor γ and C/EBPα. Diabetes 2013;62(1):115—23. https://doi.org/10.2337/db12-0295.

[13] Guo T, Marmol P, Moliner A, Björnholm M, Zhang C, Shokat KM, et al. Adipocyte ALK7 links nutrient overload to catecholamine resistance in obesity. Elife 2014;3. https://doi.org/10.7554/eLife.03245.

[14] Bu Y, Okunishi K, Yogosawa S, Mizuno K, Irudayam MJ, Brown CW, et al. Insulin regulates lipolysis and fat mass by upregulating growth/differentiation factor 3 in adipose tissue macrophages. Diabetes 2018;67(9):1761—72. https://doi.org/10.2337/db17-1201.

[15] Hashimoto O, Sekiyama K, Matsuo T, Hasegawa Y. Implication of activin E in glucose metabolism: transcriptional regulation of the inhibin/activin βE subunit gene in the liver. Life Sci 2009;85(13):534—40. https://doi.org/10.1016/j.lfs.2009.08.007.

[16] Rodgarkia-Dara C, Vejda S, Erlach N, Losert A, Bursch W, Berger W, et al. The activin axis in liver biology and disease. Mutat Res Rev Mutat Res 2006;613(2):123—37. https://doi.org/10.1016/j.mrrev.2006.07.002.

[17] Smati S, Régnier M, Fougeray T, Polizzi A, Fougerat A, Lasserre F, et al. Regulation of hepatokine gene expression in response to fasting and feeding: influence of PPAR-α and insulin-dependent signalling in hepatocytes. Diabetes Metabol 2020;46(2):129—36. https://doi.org/10.1016/j.diabet.2019.05.005.

[18] Nahmias C, Blin N, Elalouf JM, Mattei MG, Strosberg AD, Emorine LJ. Molecular characterization of the mouse beta 3-adrenergic receptor: relationship with the atypical receptor of adipocytes. EMBO J 1991;10(12):3721—7. https://doi.org/10.1002/j.1460-2075.1991.tb04940.x.

 © 2023 The Authors. Published by Elsevier GmbH. This is an open access article under the CC BY-NC-ND license (http://creativecommons.org/licenses/by-nc-nd/4.0/).

[19] Hodson L, Skeaff CM, Fielding BA. Fatty acid composition of adipose tissue and blood in humans and its use as a biomarker of dietary intake. Prog Lipid Res 2008;47(5):348—80. https://doi.org/10.1016/j.plipres.2008.03.003.

[20] Yew Tan C, Virtue S, Murfitt S, Robert LD, Phua YH, Dale M, et al. Adipose tissue fatty acid chain length and mono-unsaturation increases with obesity and insulin resistance. Sci Rep 2015;5:18366. https://doi.org/10.1038/srep18366.

[21] Le May C, Caüzac M, Diradourian C, Perdereau D, Girard J, Burnol A-F, et al. Fatty acids induce L-CPT I gene expression through a PPARalpha-independent mechanism in rat hepatoma cells. J Nutr 2005;135(10):2313—9. https://doi.org/10.1093/jn/135.10.2313.

[22] Louet JF, Chatelain F, Decaux JF, Park EA, Kohl C, Pineau T, et al. Long-chain fatty acids regulate liver carnitine palmitoyltransferase I gene (L-CPT I) expression through a peroxisome-proliferator-activated receptor alpha (PPARalpha)-independent pathway. Biochem J 2001;354(Pt 1):189—97. https://doi.org/10.1042/0264-6021:3540189.

[23] Moody L, Xu GB, Chen H, Pan Y-X. Epigenetic regulation of carnitine palmitoyltransferase 1 (Cpt1a) by high fat diet. Biochimica et Biophysica Acta (BBA) - Gene Regulatory Mechanisms 2019;1862(2):141—52. https://doi.org/10.1016/j.bbagrm.2018.12.009.

[24] Chatelain F, Kohl C, Esser V, McGarry JD, Girard J, Pegorier JP. Cyclic AMP and fatty acids increase carnitine palmitoyltransferase I gene transcription in cultured fetal rat hepatocytes. Eur J Biochem 1996;235(3):789—98. https://doi.org/10.1111/j.1432-1033.1996.00789.x.

[25] Yan Z, Yan H, Ou H. Human thyroxine binding globulin (TBG) promoter directs efficient and sustaining transgene expression in liver-specific pattern. Gene 2012;506(2):289—94. https://doi.org/10.1016/j.gene.2012.07.009.

[26] Koprulu M, Zhao Y, Wheeler E, Dong L, Rocha N, Li C, et al. Identification of rare loss-of-function genetic variation regulating body fat distribution. J Clin Endocrinol Metabol 2021;107(4):1065—77. https://doi.org/10.1210/clinem/dgab877.

[27] Reissmann E, Jörnvall H, Blokzijl A, Andersson O, Chang C, Minchiotti G, et al. The orphan receptor ALK7 and the Activin receptor ALK4 mediate signaling by Nodal proteins during vertebrate development. Gene Dev 2001;15(15):2010—22. https://doi.org/10.1101/gad.201801.

[28] Karp CL. Unstressing intemperate models: how cold stress undermines mouse modeling. J Exp Med 2012;209(6):1069—74. https://doi.org/10.1084/jem.20120988.

[29] Park J-G, Xu X, Cho S, Hur KY, Lee M-S, Kersten S, et al. CREBH-FGF21 axis improves hepatic steatosis by suppressing adipose tissue lipolysis. Sci Rep 2016;6(1):27938. https://doi.org/10.1038/srep27938.

[30] Stefan N, Schick F, Birkenfeld AL, Häring H-U, White MF. The role of hepatokines in NAFLD. Cell Metabol 2023;35(2):236—52. https://doi.org/10.1016/j.cmet.2023.01.006.

[31] Fougerat A, Schoiswohl G, Polizzi A, Régnier M, Wagner C, Smati S, et al. ATGL-dependent white adipose tissue lipolysis controls hepatocyte PPARα activity. Cell Rep 2022;39(10):110910. https://doi.org/10.1016/j.celrep.2022.110910.

[32] Lambert JE, Ramos-Roman MA, Browning JD, Parks EJ. Increased de novo Lipogenesis is a Distinct Characteristic of Individuals with Nonalcoholic Fatty Liver Disease. Gastroenterology 2014;146(3):726—35. https://doi.org/10.1053/j.gastro.2013.11.049.

[33] Gordon RS, Cherkes A. Unesterified fatty acid in human blood plasma 1. J Clin Invest 1956;35(2):206—12.

[34] Zhao M, Okunishi K, Bu Y, Kikuchi O, Wang H, Kitamura T, et al. Targeting activin receptor—like kinase 7 ameliorates adiposity and associated metabolic disorders. JCI Insight 2023;8(4). https://doi.org/10.1172/jci.insight.161229.

[35] Andersson O, Korach-Andre M, Reissmann E, Ibáñez CF, Bertolino P. Growth/differentiation factor 3 signals through ALK7 and regulates accumulation of adipose tissue and diet-induced obesity. Proc Natl Acad Sci USA 2008;105(20):7252—6. https://doi.org/10.1073/pnas.0800272105.

[36] Lee M-J. Transforming growth factor beta superfamily regulation of adipose tissue biology in obesity. Biochim Biophys Acta (BBA) - Mol Basis Dis 2018;1864(4):1160—71. https://doi.org/10.1016/j.bbadis.2018.01.025. Part A).

[37] Goebel EJ, Ongaro L, Kappes EC, Vestal K, Belcheva E, Castonguay R, et al. The orphan ligand, activin C, signals through activin receptor-like kinase 7. Elife 2022;11:e78197. https://doi.org/10.7554/eLife.78197.

[38] Keophiphath M, Achard V, Henegar C, Rouault C, Clément K, Lacasa D. Macrophage-secreted factors promote a profibrotic phenotype in human preadipocytes. Mol Endocrinol 2009;23(1):11—24. https://doi.org/10.1210/me.2008-0183.

[39] Bourlier V, Sengenès C, Zakaroff-Girard A, Decaunes P, Wdziekonski B, Galitzky J, et al. TGFbeta family members are key mediators in the induction of myofibroblast phenotype of human adipose tissue progenitor cells by macrophages. PLoS One 2012;7(2):e31274. https://doi.org/10.1371/journal.pone.0031274.

[40] Kogame M, Matsuo S, Nakatani M, Kurisaki A, Nishitani H, Tsuchida K, et al. ALK7 is a novel marker for adipocyte differentiation. J Med Invest: JMI 2006;53(3—4):238—45. https://doi.org/10.2152/jmi.53.238.

[41] Raheem J, Sliz E, Shin J, Holmes MV, Pike GB, Richer L, et al. Visceral adiposity is associated with metabolic profiles predictive of type 2 diabetes and myocardial infarction. Commun Med 2022;2(1):1—7. https://doi.org/10.1038/s43856-022-00140-5.

[42] Blüher M, Laufs U. New concepts for body shape-related cardiovascular risk: role of fat distribution and adipose tissue function. Eur Heart J 2019;40(34):2856—8. https://doi.org/10.1093/eurheartj/ehz411.

[43] Arner P, Rydén M. Fatty acids, obesity and insulin resistance. Obes Facts 2015;8(2):147—55. https://doi.org/10.1159/000381224.

[44] Morigny P, Houssier M, Mouisel E, Langin D. Adipocyte lipolysis and insulin resistance. Biochimie 2016;125:259—66. https://doi.org/10.1016/j.biochi.2015.10.024.

[45] Boden G, Chen X. Effects of fat on glucose uptake and utilization in patients with non-insulin-dependent diabetes. J Clin Investig 1995;96(3):1261—8. https://doi.org/10.1172/JCI118160.

[46] Girousse A, Tavernier G, Valle C, Moro C, Mejhert N, Dinel A-L, et al. Partial inhibition of adipose tissue lipolysis improves glucose metabolism and insulin sensitivity without alteration of fat mass. PLoS Biol 2013;11(2):e1001485. https://doi.org/10.1371/journal.pbio.1001485.

[47] Adam RC, Pryce DS, Lee JS, Zhao Y, Mintah IJ, Min S, et al. Activin E—ACVR1C cross talk controls energy storage via suppression of adipose lipolysis in mice. Proc Natl Acad Sci USA 2023;120(32):e2309967120. https://doi.org/10.1073/pnas.2309967120.

[48] Wang H, Yang H, Shivalila CS, Dawlaty MM, Cheng AW, Zhang F, et al. One-step generation of mice carrying mutations in multiple genes by CRISPR/Cas-mediated genome engineering. Cell 2013;153(4):910—8. https://doi.org/10.1016/j.cell.2013.04.025.

[49] Harms MJ, Ishibashi J, Wang W, Lim H-W, Goyama S, Sato T, et al. Prdm16 is required for the maintenance of Brown adipocyte identity and function in adult mice. Cell Metabol 2014;19(4):593—604. https://doi.org/10.1016/j.cmet.2014.03.007.

[50] Hausman DB, Park HJ, Hausman GJ. Isolation and culture of preadipocytes from rodent white adipose tissue. Methods Mol Biol 2008;456:201. https://doi.org/10.1007/978-1-59745-245-8_15. 19.

[51] Tsagkaraki E, Nicoloro SM, DeSouza T, Solivan-Rivera J, Desai A, Lifshitz LM, et al. CRISPR-enhanced human adipocyte browning as cell therapy for metabolic disease. Nat Commun 2021;12(1):6931. https://doi.org/10.1038/s41467-021-27190-y.

[52] Toni LS, Garcia AM, Jeffrey DA, Jiang X, Stauffer BL, Miyamoto SD, et al. Optimization of phenol-chloroform RNA extraction. MethodsX 2018;5:599—608. https://doi.org/10.1016/j.mex.2018.05.011.

[53] Pfaffl MW. A new mathematical model for relative quantification in real-time RT—PCR. Nucleic Acids Res 2001;29(9):e45.

 © 2023 The Authors. Published by Elsevier GmbH. This is an open access article under the CC BY-NC-ND license (http://creativecommons.org/licenses/by-nc-nd/4.0/).